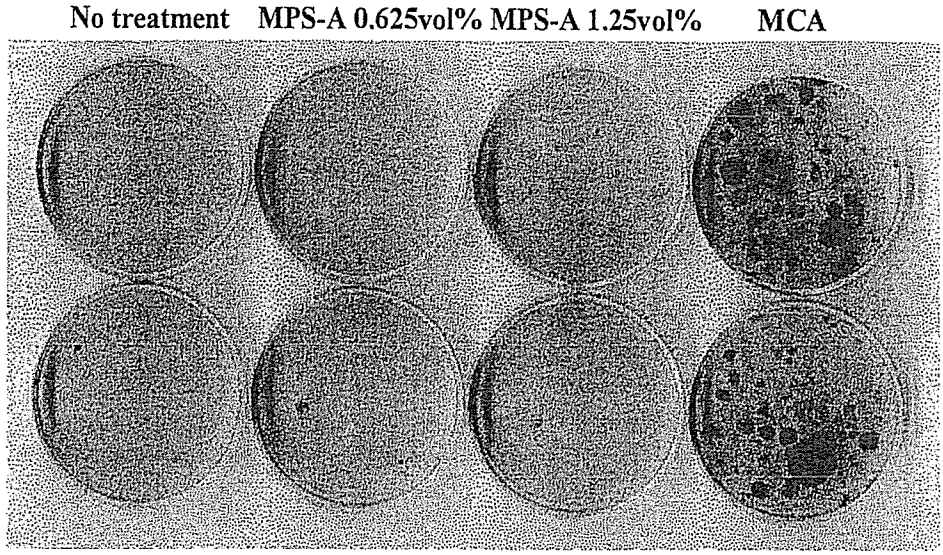

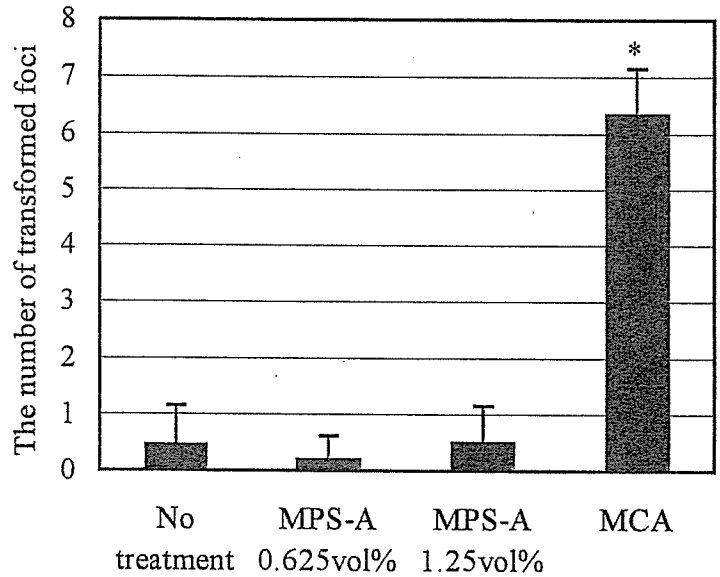

Figure 7. Two-stage Balb3T3 cell transformation test for MPS-A. Each bar represents the mean ± standard deviation of 15 determinations in graph. Transformed foci were deeply stained by Giemsa staining, as shown in the dishes (upper photos). All data are expressed as the mean ± standard deviation of 15 determinations and treated statistically with Tukey's (a) multiple-comparison test. *$p <$ 0.05, significant difference in comparison with no treatment of control. Experiments were repeated at least two times.

Then, the time course for recovery from MPS-A–induced inhibition of GJIC was examined (Figure 5). In this experiment, confluent cultures of RC4 cells were treated with MPS-A (0.625 vol%) or poloxamine (0.125%) for 1 h under standard conditions. After that, the medium was replaced with fresh ME10 and the distance of dye migration was measured at appropriate times (0–72 h after treatment). As a result, the recovery of GJIC was time dependent and reached former levels in 24 h [Tukey's(a) multiple-comparison test; $p < 0.01$]. The time course of recovery after exposure for 24 h is also shown in Figure 5. Similarly, time-dependent restoration was observed after 4 h, and complete recovery was established after approximately 24 h [Tukey's(a) multiple-comparison test; $p < 0.01$]. These results showed that the method of inhibition induced by MPS-A was reversible.

Western-blotting analysis was conducted for connexin-43, which is a major protein constituting the gap junctional channels of these cells, to examine whether MPS-A caused changes in the amounts of this protein, in addition to the degree of its phosphorylation after treatment of RC4 cells

with MPS-A (Figure 6). The three typical bands (P_0, P_1, P_2) of connexin-43 corresponding to three forms of connexin-43 that have been identified in other cells, were detected in untreated RC4 cells. They were separated according to the degree of phosphorylation state; the P_0 represents nonphosphorylated connexin-43, and P_2 represents a much higher phosphorylated state than P_1. After 30 min of incubation with 0.625 vol% MPS-A in RC4 cells under standard conditions, the total level of connexin-43 in the cells was reduced. Importantly, decreasing amounts of P_2 were observed compared with the amounts in control cells. After 24 h incubation, the total level of connexin-43 was approximately restored and the amounts of P_2 were also restored. Therefore, it was suggested that this short-time decrease in the amount of connexin-43 was ascribed to the inhibitory action on GJIC. Moreover, the inhibitory action might be induced by the change in connexin-43 to the dephosphorylated form, such as the P_2 level, to P_1 or P_0. It was reported that the phosphorylated state of connexin-43 is important for its accurate assembly and distribution in cells.[4] Probably, connexin-43 on RC4 was not phosphorylated to the P_2 level by MPS-A exposure, so that the gap junction could not assemble, which was ascribed to the inhibitory action on GJIC. To clarify this, the localization of connexin-43 is currently being evaluated by immunostaining.

The results in the present study supported the idea that the change in connexin-43 expression is the major cause of the change in GJIC function on the cornea when the cells were exposed to MPS-A. The method of the inhibitory action in RC4 was reversible, but it took approximately 24 h for the GJIC to be restored completely. Many contact lens users typically wear contact lenses for over 12 h, and in some cases hydrogel contact lenses swell or absorb the ingredients of MPS-A. Therefore, there might be a situation that some MPS-A or its ingredient remains on the surface of contact lenses, which suggests that the corneas of wearers are exposed directly to them. In this case, MPS-A or its ingredients might cause disorder to the GJIC on the cornea, and so the phenomenon, which is always a disorder of the homeostasis of the cornea, is in a stationary state. It is possible that this state may lead to poor resistance for diseases. The finding that several diseases originated from the lack or damage of connexin[17] supports this kind of risk. In addition, recent immunohistochemical and immunoblotting studies showed that there was less connexin-43 in rat corneas exposed to MPS-A than in cornea exposed to MPS-B and C *in vivo* (data not shown). It was suggested that there is a disorder of the homeostasis of the cornea exposed to MPS-A *in vivo,* because it was suggested that the quantity and function of the gap junction is linked to the abundance of connexin-43. It is possible that the same phenomenon occurs on the corneas of humans (MPS-A users).

To study the tumor activity of MPS-A, a Balb3T3 two-stage cell transformation assay was conducted (Figure 7). No significant difference was found between ME10 containing MPS-A 1.25 vol%, 0.625 vol%, and negative controls (ME10 alone) [Tukey's(a) multiple-comparison test; $p > 0.05$]. These results suggested that the tumor-promoting potency of MPS-A is low, compared with positive controls (MCA) or phorbol esters that are well known as tumor-promoting agents.[18] However, there is definitely a disorder of GJIC on cells exposed to MPS-A, which causes a dysfunction to the homeostasis of the cornea. Recently, it was reported that disruption of connexin leads to cataractogenesis in mice.[19] So, it is possible that exposing the cornea to MPSs, which inhibit GJIC, can have a severe influence on the homeostasis of the cornea and induce cataractogenesis or other diseases.[20]

The present study tried to introduce methods to evaluate the effects on GJIC as a criterion for safety for the cornea. These methods could detect inhibitory activities of GJIC at non-cytotoxic concentrations. Compared with previous methods, this one is thought to be more suitable for evaluating the long-term safety of MPS.

The authors thank Yuki Suita for her technical assistance.

REFERENCES

1. Yamasaki H, Mesnil M, Omori Y, Mironov N, Krutovskikh V. Role of blocked gap junctional intercellular communication in non-genotoxic carcinogenesis. Toxicol Lett 1995;82–83:701–706.
2. Bennett MV, Barrio LC, Bargiello TA, Spray DC, Hertzberg E, Saez JC. Gap junctions: New tools, new answers, new questions. Neuron 1991;6:305–320.
3. Kumar NM, Gilula NB. The gap junction communication channel. Cell 1996;84:381–388.
4. Yamasaki H. Role of disrupted gap junctional intercellular communication in detection and characterization of carcinogens. Mutat Res 1996;365:91–105.
5. Tsuchiya T. Detection of tumor-promoting activities in biomaterials using in vitro cell culture methods. Kobunshi Ronbunshu 1998;55:314–322.
6. Dong Y, Roos M, Gruijters T, Donaldson P, Bullivant S, Beyer E, Kistler J. Differential expression of two gap junction proteins in corneal epithelium. Eur J Cell Biol 1994;64:95–100.
7. Matic M, Petrov IN, Rosenfeld T, Wolosin JM. Alterations in connexin expression and cell communication in healing corneal epithelium. Invest Ophthalmol Vis Sci 1997;38:600–609.
8. Petridou S, Masur SK. Immunodetection of connexins and cadherins in corneal fibroblasts and myofibroblasts. Invest Ophthalmol Vis Sci 1996;37:1740–1748.
9. Joyce NC, Harris DL, Zieske JD. Mitotic inhibition of corneal endothelium in neonatal rats. Invest Ophthalmol Vis Sci 1998; 39:2572–2583.
10. Sumide T, Tsuchiya T. Evaluation of chemical disinfectants for hydrogel contact lenses by metabolic cooperation assay. J Jpn Soc Biomater 2001;119:93–97.
11. El-Fouly MH, Trosko JE, Chang CC. Scrape-loading and dye transfer. A rapid and simple technique to study gap junctional intercellular communication. J Exp Cell Res 1987;168:422–430.
12. Park JU, Tsuchiya T. Increase in gap-junctional intercellular communications (GJIC) of normal human dermal fibroblasts (NHDF) on surfaces coated with high-molecular-weight hyaluronic acid (HMW HA). J Biomed Mater Res 2002;60:541–547.
13. Ichikawa A, Tsuchiya T. Reversion of transformed phenotype of polyetherurethane-induced tumor cells by Cx43 transfection. Animal Cell Technol Basic Appl Aspects 2002;12:269–273.

14. IARC/NCI/EPA Working Group. Cellular and molecular mechanisms of cell transformation and standardization of transformation assays of established cell lines for the prediction of carcinogenic chemicals: Overview and recommended protocols. Cancer Res 1985;45:2395–2399.
15. Yotti LP, Chang CC, Trosko JE. Elimination of metabolic cooperation in Chinese hamster cells by a tumor promoter. Science 1979;206:1089–1091.
16. Tsuchiya T, Hata T, Nakamura A. Studies on the tumor-promoting activity of biomaterials: Inhibition of metabolic cooperation by polyetherurethane and silicone. J Biomed Mater Res 1995;29:113–119.
17. Donaldson P, Eckert R, Green C, Kistler J. Gap junction channels: New roles in disease. Histol Histopathol 1997;12:219–231.
18. Yamasaki H, Krutovskikh V, Mesnil M, Tanaka T, Zaidan-Dagli ML, Omori Y. Role of connexin (gap junction) genes in cell growth control and carcinogenesis. C R Acad Sci III 1999; 322:151–159.
19. Gong X, Li E, Klier G, Huang Q, Wu Y, Lei H, Kumar NM, Horwitz J, Gilula NB. Disruption of alpha3 connexin gene leads to proteolysis and cataractogenesis in mice. Cell 1997;91:833–843.
20. Suzuki K, Tanaka T, Enoki M, Nishida T. Coordinated reassembly of the basement membrane and junctional proteins during corneal epithelial wound healing. Invest Ophthalmol Vis Sci 2000;41:2495–2500.
21. Trosko JE, Ruch RJ. Cell–cell communication in carcinogenesis. Frontiers Biosci 1998;3:208–236.

BIOCOMPATIBLE BIOMATERIALS FOR THE HUMAN CHONDROCYTE DIFFERENTIATION ESTIMATED BY RT-PCR METHOD.

TOSHIE TSUCHIYA, MASAMUNE SAKAI*, HIROYUKI IKEDA*, TADAHIKO MASHINO** AND YASMIN BANU.

National Institute of Health Sciences, Division of Medical Devices, 1-18-1 Kamiyoga, Setagaya-ku, Tokyo 158-8501, Japan.

**UBE Industries, LTD. Polymer Laboratory (Chiba), 8-1, Goi Minamikaigan, Ichihara City, Chiba 290-0045, Japan*

***Kyoritsu College of Pharmacy,1-5-30 shibakouen, minato-ku, Tokyo 105-8512, Japan.*

Abstract

Biocompatibility of the biomaterials for the differentiation of the human articular chondrocytes were estimated by reverse transcription-polymerase chain reaction (RT-PCR). We used five biodegradable polymers for culturing with human articular chondrocytes. In addition to these five materials, we also estimated aquous type of fullerene, namely C60 dimalonic acid (C60DMA). Cultures were carried out using micromass culture method for 4 weeks. Collagen type II, aggrecan and connexin43 gene levels were estimated using RT-PCR methods. Among the biomaterials, Poly glycolic acid (PGA) showed the highest expression level of the collagen type II gene. On the contraty, C60DMA showed the lowest expression level among six kinds of test substances. In the case of the aggrecan gene, PGA also showed the highest levels, and C60DMA showed the lowest ones. However, the expression patterns of the connexin 43 gene were different from previous two genes. Using the multi regression analysis was carried out between differentiation and these three gene expression levels. There was a high correlation between cellular differentiation and three gene expression levels.

1. Introduction

Properties of degradation of scaffolds are the important character in the long-term success of a tissue-engineered cartilage construct. The biodegradable polymers hold the additional advantage that the cartilage tissue, with the biodegradation of the polymers, may gradually replace the space occupied by the scaffolds. Extensive studies have been carried out using bioreabsorbable materials. However, most of those studies used animal cells, whereas little information is available on the chondrogenic effects of these materials with human articular chondrocytes (HAC). The biocompatibility of the biodegradable polymers using human articular cartilage in a micromass culture system was studied. In the present in vitro micromass study, we investigated the biocompatibility of a synthetic biodegradable materials and a fullerene derivative of C60 dimalonic acid (C60DMA) as the indication of the cellular proliferation, differentiation and the expression level of 3 genes such as collagen type II, aggrecan and connexin43, estimated by RT-PCR method.

K. Yagasaki et al. (eds.), Animal Cell Technology: Basic & Applied Aspects, Volume13, 475-479.

2. Materials and Methods

Cell and Materials

Chondrocyte growth medium and HAC were commercially obtained from BioWhittaker, Inc. (Walkersville, MD, USA). Chondrocytes growth medium contains bovine insulin, basic fibroblast growth factor, insulin like growth factor-1, transferring, gentamicin sulfate and fetal bovine serum (5% v/v). PGA (Mw = 3,000) and PLGA (Mw = 5,000) were purchased from Nakalai Tesque Inc. (Kyoto, Japan) and, PGCL (Mw = 3,000) was from Taki Chemical Co (, Japan). P(LA-CL)25 Mw = (10,000) , PCL (Ti) (Mw = 130,000) and fullerene C60-dimalonic acid (C60 DMA) were synthesized in our laboratoty.

Cell culture

In vitro high-density micromass cultures of HAC were initiated by spotting $4x10^5$ cells in 20 μl of medium onto each well of 12-well microplates for tissue culture (Costar ® Type 3513, Corning Co. Ltd., NY, USA) and PCL(Ti) coated glass wells (diameter, 22mm). After two hours of cell spotting in a 5 % CO_2 incubator at 37°C, the wells were flooded with chondrocyte culture media (2 ml/well). Media were supplemented with DMSO (0.8 μl/ml), PGA (50 μg/ml), PGCL (50 μg/ml), PLGA (50 μg/ml), P(LA-CL)25 (50 μg/ml), and fullerene C60 DMA (60 μg/ml), respectively. HAC cultured on tissue culture polystyrene but not exposed to any biomaterials served as a control. The media were changed in every 3 days and the cultures were continued for 4 weeks.

Proliferation assay

Cell proliferation was quantitatively measured by alamar blue (Biosource, International, Inc, Camarillo, CA) assay after 4 weeks of culture as previously described.[1]

Differentiation assay

Proteoglycans are typical contents of the cartilage matrix. The extent of chondrogenesis was determined by staining the cartilage specific proteoglycans with alcian blue (Wako Pure Chemical Industries, Ltd., Osaka, Japan) as previously described.[2]

RNA harvest

After the designated 4 weeks culture period, RNA was extracted from all matrices except PCL(Ti) matrix. For PCL(Ti) matrix, we did not have enough samples for RNA harvest as cells from 50 % of the cultured wells were detached over night following cell spotting. Total celluar RNA was extracted from cultured cells of four wells (for each material) in 0.5 ml Trizol reagent (Life Technologies, Inc., Frederick, MD, USA) according to manufacturer's instruction.

Reverse transcription (RT) and polymerase chain reaction (PCR)

The matrix molecules probed as part of this study was collagen type II and aggrecan. The gap junction protein gene of Cx43 was also studied. The single strand cDNA was prepared from 1 μg of total RNA by reverse transcription (RT) using a commercially available First-Strand cDNA synthesis kit (Amersham Pharmacia Biotech, Uppsala, Sweden). After proper optimization of PCR condition, subsequent PCR was performed with 4 μg of cDNA in a 20 μl reaction mixture (10 x PCR buffer 2 μl,

dNTP 1.6 μl, forward and reverse, each primer 0.4 μl, Taq DNA polymerase 0.1 μl and rest of the amount of distilled water). The codon sequence used for the primer sets was as follows:

Collagen type II: forward 5'-GGCAATAGCAGGTTCACGTACA-3'
reverse 5'-CGATAACAGTCTTGCCCCACTT-3'

Aggrecan: forward 5'-TCGAGGACAGCGAGGCC-3'
reverse 5'-TCGAGGGTGTAGCGTGTAGAGA-3'.

Connexin 43 (Homo Sapiens):
forward 5'-ATGGGTGACTGGAGCGCCTTAGGCAAACTC-3'
reverse 5'- GACCTCGGCCTGATGACCTGGAGATCTAG -3'

The polymerization of GAPDH was accomplished by 25 cycles with the corresponding PCR program. Electrophoresis of PCR products was done on 3% agarose gel for the visualization of collagen type II and aggrecan and, on 1% agarose gel for Cx43 after staining with SYBR Green I (BioWhittaker Molecular Applications, Rockland, ME, USA). The relative intensity of signals from each lane was analyzed with a computerized scanner. For relative quantitation, the signal intensity of each lane was standardized to that of a housekeeping gene, glyceraldehydes-3-phosphate dehydrogenase (GAPDH):

forward 5'-CCCATCACCATCTTCCAGGAGCGAGA-3'
reverse 5'-TGGCCAAGGTCATCCATGACAACTTTGG-3'.

3. Results

Cell proliferation assay

The cell proliferations of PGA, PGCL and PLGA were fairly parallel as that of control cell proliferation. The cell proliferation of P(LA-CL)25, PCL(Ti) and fullerene C-60 DMA were significantly inhibited as compared to control. The values of cell proliferation for the samples exposed to PGA, PGCL, PLGA, P(LA-CL)25, PCL(Ti) and fullerene C-60 were 101, 102, 104, 93, 84, and 93 %, respectively.

Proteoglycan synthesis

Intensity of alcian blue staining was found to be higher in PGA, PGCL and PLGA containing cultures than that was found with the control culture. Among the biomaterials, PGA caused a significant 3.1 fold increase of cell differentiation when compared to control ($p < 0.05$).

Extracellular matrix genes expression

RT-PCR analysis showed that all matrices consistently expressed collagen type II gene and PGA matrix had the strongest induction. Slight increase expressions of collagen type II gene were noted with PGCL and PLGA matrices. Expression of collagen type II gene in P(LA-CL)25 was faint and in fullerene C60 DMA was almost nil. PGA matrix showed the strongest induction of aggrecan gene. Aggrecan gene expressions were decreased in PLGA and P(LACL)25 matrices.

Expression of gap junction protein connexin 43 gene

PGA induced the highest level of Cx43 mRNA expression and moderate level of expression was noticed in PLGA treated culture. A faint expression in P(LA-CL)25 and almost nil expression in flurrene C60 DMA treated cultures were observed.

Multi-regression analysis

Using the multi regression analysis, correlation was investigated between the differentiation estimated by alcian blue method and three genes expression levels. There was a high correlation between the cellular differentiation and three gene expression (correlation coefficient is 0.96) (Fig.1). Especially, two kinds of expression levels of aggrecan, and connexin 43 genes, were found to be critical factors for estimating the extent of cellular differentiation of human articular chondrocytes(Fig. 1).

4. Discussion

During differentiation, chondrocytes secrete extracellular matrix (ECM) molecules characteristic of cartilage, such as type II collagen, aggrecan, and link protein, offering an environment that preserves the chondrocyte phenotype. Therefore, chondrocyte are defined both by their morphology and ability to produce these characteristic ECM. Collagen type II is regarded as the most important component among the ECM molecules. Previous study detected type II collagen as early as 7 days after beginning 3-D culture and at 21 days, the matrix of the entire aggregate contained type II collagen.[3] Among the ECM molecules, aggrecan is a major proteoglycan[4] and had been reported that in chick cartilage, aggrecan starts to be expressed at embryonic day 5 in limb rudiments, continues through the entire period of chondrocyte development, and remains a biochemical marker of the cartilage phenotype thereafter.[5] In this study, we have well demonstrated cell differentiation with the formation of cartilaginous nodules on culture plate, by alcian blue staining, which is commonly used for identification of cartilage, and by expression of ECM molecules collagen type II and aggrecan. The morphology after the designated culture period revealed that cells aggregated on the culture plate and resulted in the formation of cartilaginous nodules. The greatest cell differentiation, 3.1-fold increase of the controls was found in the sample treated with PGA. The potencies of cell differentiation after 4 weeks of culture from most to least were in the following order; PGA>> PLGA > PGCL > Cont. = DMSO > P(LA-CL)25 = PCL(Ti) >> fullerene C60 DMA. The increased cell differentiation with PGA and PLGA matrices are in agreement with our previous findings in micromass culture system[1], however, in this study we have included the matrix genes expression of these materials. Results of the present study confirmed PGA and PLGA as useful scaffolding matrices for cartilage tissue engineering, and knowledge with other matrices will further contribute to develop improved cartilaginous constructs for future clinical implants. In this study, RT-PCR analysis showed that the mRNA level of x43 gene expression was consistent with the chondrogenic differentiation in the presence of different biomaterials. Our findings of Cx43 expression by chondrocytes are in agreement of previous study that reported expression of functional gap junctions by chondrocytes isolated from adult articular cartilage[6]. Gap junction mediated intercellular communication is critically involved in the development of cartilage during differentiation[7].

In this study, the data of cell differentiation by alcian blue and, observed expression of collagen type II, aggrecan and Cx43 suggest that the process of cell differentiation might be due to the interconnection of cells by means of gap junction along with other molecular mechanism. However, the specific association of gap junction in the process of chondrogenic differentiation and the cell signaling processes remains unexplored. Future studies are required to analyze the specific role that the gap junction proteins have in chondrocyte differentiation.

5. Acknowledgement

We are grateful to the support of Health and Labour Sciences Research Grants, Research on Advanced Medical Technology, Ministry of Health, Labour and Welfare and Japan Health Sciences Foundation.

6. References

1. Rahman MS, Toshie Tsuchiya. Enhancement of chondrogenic differentiation of human articular chondrocytes by biodegradable polymers. Tissue Engineering; 2001;7:781-790.
2. Tsuchiya T, Yamakoshi YN, Miyata N. A novel promoting action of fullerene C60 on the chondrogenesis in rat embryonic limb bud cell culture system. Biochem Biophys Res Commun. 1995;206:885-894.
3. Johnstone B, Hering TM, Caplan AI, Goldberg VM, Yoo JU. In vitro chondrogenesis of bone marrow-derived mesenchymal progenitor cells. Exp Cell Res. 1998;23:265-272.
4. Watanabe H, Yamada Y, Kimata K. Roles of aggrecan, a large chondroitin sulfate proteoglycan, in cartilage structure and function. J Biochem (Tokyo). 1998;124: 687-693.
5. Schwartz NB, Domowicz M, Krueger RC Jr, Li H, Mangoura D. Brain aggrecan. Perspect Dev Neurobiol 1996;3:291-306
6. Donahue HJ, Guilak F, Vander Molen MA, McLeod KJ, Rubin CT, Grande DA, Brink PR. Chondrocytes isolated from mature articular cartilage retain the capacity to form functional gap junctions. J Bone Miner Res 1995;10:1359-1364
7. Coelho CN, Kosher RA. Gap junctional communication during limb cartilage differentiation. Dev Biol 1991;144:47-53

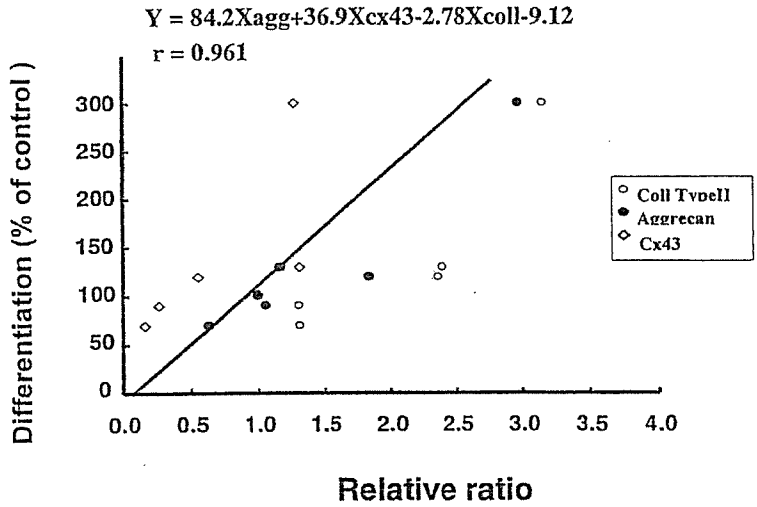

Fig.1.Relationship between the differentiation and the expression levelS of three genes of collagen typeII, aggrecan and connexin43 using multi-regression analysis.

J|A|C|S
ARTICLES
Published on Web 09/24/2003

Active Oxygen Species Generated from Photoexcited Fullerene (C_{60}) as Potential Medicines: $O_2^{-\bullet}$ versus $^1O_2$

Yoko Yamakoshi,*,† Naoki Umezawa,‡ Akemi Ryu,§ Kumi Arakane,§ Naoki Miyata,† Yukihiro Goda,† Toshiki Masumizu,|| and Tetsuo Nagano‡

Contribution from the Division of Organic Chemistry, National Institute of Health Sciences, 1-18-1 Kamiyoga, Setagaya, Tokyo 158-8501, Japan; Graduate School of Pharmaceutical Sciences, The University of Tokyo, 7-3-1 Hongo, Bunkyo, Tokyo 113-0033, Japan; Research Laboratory, KOSÉ Corporation, 1-18-4 Azusawa, Itabashi, Tokyo 174-0051, Japan; and Application and Research Center, JEOL, 3-1-2 Musashino, Akishima, Tokyo 196-8558, Japan

Received April 10, 2003; E-mail: yamakosh@nihs.go.jp; yamakoshi@chem.ucsb.edu

Abstract: To characterize fullerenes (C_{60} and C_{70}) as photosensitizers in biological systems, the generation of active oxygen species, through energy transfer (singlet oxygen $^1O_2$) and electron transfer (reduced active oxygen radicals such as superoxide anion radical $O_2^{-\bullet}$ and hydroxyl radical •OH), was studied by a combination of methods, including biochemical (DNA-cleavage assay in the presence of various scavengers of active oxygen species), physicochemical (EPR radical trapping and near-infrared spectrometry), and chemical methods (nitro blue tetrazolium (NBT) method). Whereas $^1O_2$ was generated effectively by photoexcited C_{60} in nonpolar solvents such as benzene and benzonitrile, we found that $O_2^{-\bullet}$ and •OH were produced instead of $^1O_2$ in polar solvents such as water, especially in the presence of a physiological concentration of reductants including NADH. The above results, together with those of a DNA cleavage assay in the presence of various scavengers of specific active oxygen species, indicate that the active oxygen species primarily responsible for photoinduced DNA cleavage by C_{60} under physiological conditions are reduced species such as $O_2^{-\bullet}$ and •OH.

Introduction

Photodynamic therapy (PDT) is an important approach to cancer treatment and is emerging as an antimicrobial chemotherapy with particular promise for the treatment of multidrug resistant pathogens. In a typical course of PDT, the combination of a photosensitizing agent and focused irradiation is used to elicit specific, controlled production of reactive species in a localized area, leading to cell destruction through several pathways, of which one of the most important is DNA strand cleavage. By using highly focused light irradiation, PDT has the potential to act specifically at the desired site of action with low levels of collateral damage to healthy cells.

Typical photosensitizers used for PDT are aromatic molecules, which can efficiently form a long-lived triplet excited state and which have the potential to generate highly reactive oxygen species. The ideal drug for PDT should have a high quantum yield to form reactive species, a long wavelength of absorption, and low toxicity in the nonilluminated state. While the majority of clinically employed photosensitizers for PDT are porphyrin-based, associated side effects and the search for more efficient therapeutic agents have led numerous groups, including our own, to investigate the potential of fullerene (C_{60} and C_{70}) derivatives as novel PDT drugs.[1] Such molecules are particularly attractive due to their long wavelength of absorption ((S−S absorption: 530, 920 nm (C_{60}); 570, ~740, ~900 nm (C_{70}). T−T absorption: 400, 740 nm (C_{60}); 525, 575, 960 nm (C_{70})),[2] high quantum yield (1.0 based on generation of singlet oxygen, $^1O_2$),[3−5] and lack of acute toxicity, except in rare cases,[6] in the absence of light. Despite these advantages, progress in the development of fullerene-based agents for PDT has been hampered by two major obstacles: (1) the low solubility of fullerenes in biologically relevant media[7] and (2) the uncertainty about the mechanism of action of photoexcited fullerenes in biological systems.

To realize the potential of these promising compounds, we have sought to overcome both of these limitations. In particular, our discovery of a novel approach to the effective solubilization of fullerenes in aqueous, physiologically relevant media[8] has enabled the study of the mechanism and biological activity of photoexcited fullerenes, leading to the discovery of DNA strand cleaving activity,[9] hemolytic activity,[10] antimicrobial photodynamic therapy[11] and cytotoxicity,[12,13] and, in the absence of irradiation, a chondrogenesis-promoting effect[14,15] and glutathione *S*-transferase-inhibitory activity.[16] The readily availability of aqueous fullerene solutions also led to the first mechanistic study of active oxygen generation by underivatized photoexcited fullerenes *in aqueous media*, leading to the

† National Institute of Health Sciences, Japan.
‡ Graduate School of Pharmaceutical Sciences, The University of Tokyo.
§ Research Laboratory, KOSÉ Corporation.
|| Application and Research Center, JEOL.

(1) For reviews on photophysical properties of fullerenes, see: (a) Guldi, D. M.; Prato, M. *Acc. Chem. Res.* **2000**, *33*, 695−703. (b) Guldi, D. M. *Chem. Commun.* **2000**, 321−327. (c) Guldi, D. M.; Kamat, P. V. In *Fullerenes Chemistry, Physics, and Technology*; Kadish, K. M., Ruoff, R. S., Eds.; Wiley: New York, 2000; pp 225−281.

10.1021/ja0355574 CCC: $25.00

discovery of superoxide ($O_2^{-\bullet}$) and hydroxyl radical (•OH), rather than the expected singlet oxygen ($^1O_2$), as the active species for DNA cleavage activity.[17]

We now present a full account of our studies documenting the specific generation of $O_2^{-\bullet}$ and •OH by photoexcited C_{60} solubilized by detergent in aqueous solutions, which are in marked contrast with previous explanations for the observed biological activity of photoexcited C_{60}. Prior studies on photoexcited C_{60}, which were performed in organic solvents or on water-soluble C_{60} derivatives, have suggested a critical role of $^1O_2$ generation and subsequent DNA cleavage.[18-20] Further experimentation on related derivatives, however, cast doubt on the role of $^1O_2$ in mediating the observed biological activity. In this regard, An et al. demonstrated that, while the DNA-cleaving activity of eosine derivatives (well-known $^1O_2$ generators) was suppressed by the addition of $^1O_2$ trapping reagents, the DNA-cleaving ability of photoexcited C_{60} was unaffected by such $^1O_2$ traps.[21]

The photochemical properties of fullerenes have been well studied. The first study of this type, reported by Foote and coworkers, described the appearance of an excited state of C_{60} ($^1C_{60}$* and $^3C_{60}$*) that subsequently afforded $^1O_2$ through an energy transfer mechanism (type II pathway, eq 1).[3] A closely

$$^1C_{60} \xrightarrow{h\nu} {}^1C_{60}^* \xrightarrow{\text{ISC}} {}^3C_{60}^* \xrightarrow{{}^3O_2 \rightarrow {}^1O_2} {}^1C_{60} \quad (1)$$

related study on C_{70} was subsequently reported.[4] Almost simultaneously, Wasielewski et al. detected triplet-excited states of C_{60} and C_{70} ($^3C_{60}$* and $^3C_{70}$*) by an EPR method.[22] Other investigators extended these findings to the study of type II energy transfer by photoexcitation of fullerenes.[23]

Electron transfer (type I pathway, eq 2) reactions of photoexcited fullerene have been reported.[2] In 1991, Krusic et al. reported the generation of $C_{60}^{-\bullet}$ by photolysis in the presence of an electron donor.[2a] Shortly thereafter, Foote et al. described the generation of $C_{60}^{-\bullet}$ by photoirradiation of C_{60} in the presence of amines and reported the high first electron-reducing voltage of $^3C_{60}$* (E_1 = +1.14 V vs SCE in PhCN, $^1C_{60}$: E_1 = −0.42 V vs SCE in PhCN).[2b]

$$^1C_{60} \xrightarrow{h\nu} {}^1C_{60}^* \xrightarrow{\text{ISC}} {}^3C_{60}^* \xrightarrow[E_{red} = +1.14\ \text{V}]{\text{e}^-\text{-donor}} C_{60}^{-\bullet} \quad (2)$$

In the present paper, we report the generation of active oxygen species from photoexcited fullerenes through both type I and II pathways, in solvents with a range of polarity values and we evaluate the contributions of these active species to photoinduced DNA cleavage under physiological conditions.

Results and Discussion

To clarify the active species principally responsible for the DNA cleavage upon photoirradiation, we employed biochemical (DNA-cleavage assay), chemical (NBT method), and physicochemical methods (EPR spin-trapping and near-infrared spectroscopy).

DNA Cleavage. First, we examined the DNA-cleavage activity of C_{60} and C_{70} to establish the effects of visible light, reductants, and initiator or quencher of $O_2^{-\bullet}$ and $^1O_2$. The widely used assay with pBR322 supercoiled DNA was employed. According to our previous report,[8] C_{60} and C_{70} were solubilized in water with poly(vinylpyrrolidone) (PVP). Figure 1 shows that

(2) (a) Krusic, P. J.; Wasserman, E.; Parkinson, B. A.; Malone, B.; Holler, E. R., Jr.; Keizer, P. N.; Morton, J. R.; Preston, K. F. *J. Am. Chem. Soc.* **1991**, *114*, 6274−6275. (b) Arbogast, J. W.; Foote, C. S.; Kao, M. *J. Am. Chem. Soc.* **1992**, *114*, 2277−2279. (c) Brezová, V.; Stasko, A.; Rapta, P.; Domschke, G.; Bartl, A.; Dunsch, L. *J. Phys. Chem.* **1995**, *99*, 16234−16241. (d) Brezová, V.; Guegel, A.; Rapta, P.; Stasko, A. *J. Phys. Chem.* **1996**, *100*, 16232−16237. (e) Stasko, A.; Brezová, V.; Rapta, P.; Biskupic, S.; Dinse, K.-P.; Gügel, A. *Res. Chem. Intermed.* **1997**, *23*, 453−478. (f) Ruebsam, M.; Dinse, K.-P.; Plueschau, M.; Fink, J.; Krätschmer, W.; Fostiropoulos, K.; Taliani, C. *J. Am. Chem. Soc.* **1992**, *114*, 10059−10061. (g) Hwang, K. C.; Mauzerall, D. *J. Am. Chem. Soc.* **1992**, *114*, 9705−9806. (h) Hwang, K. C.; Mauserall, D. *Nature*, **1993**, *361*, 138−141. (i) Osaki, H.; Tai, Y.; Tazawa, M.; Yanemura, S.; Inukai, K.; Ishiguro, K.; Sawaki, Y.; Saito, Y.; Shinohara, H.; Nagashima, H. *Chem. Lett.* **1993**, 789−792. (j) Imahori, H.; Cardoso, S.; Tatman, D.; Lin, S.; Noss, L.; Seely, G. R.; Sereno, L.; de Silber, J. C.; Moore, T. A.; Moore, A. L.; Gust, D. *Photochem. Photobiol.* **1995**, *62*, 1009−1014. (k) Williams, R. M.; Zwier, J. M.; Verhoeven, J. W. *J. Am. Chem. Soc.* **1995**, *117*, 4093−4099. (l) Imahori, H.; Hagiwara, K.; Aoki, M.; Akiyama, T.; Taniguchi, S.; Okada, T.; Shirakawa, M.; Sakata, Y. *J. Am. Chem. Soc.* **1996**, *118*, 11771−11782. (m) Mikami, K.; Matsumoto, S.; Ishida, A.; Takamura, S.; Suenobu, T.; Fukuzumi, S. *J. Am. Chem. Soc.* **1995**, *117*, 11134−11141. (n) Kuciauskas, D.; Lin, S.; Seely, G. R.; Moore, A. L.; Moore, T. A.; Gust, D.; Drovetskaya, T.; Reed, C. A.; Boyd, P. D. W. *J. Phys. Chem.* **1996**, *100*, 15926−15932. (o) Guldi, D. M.; Asmus, K.-D. *J. Phys. Chem.* **1997**, *101*, 1472−1481. (p) Fukuzumi, S.; Suenobu, T.; Kawamura, S.; Ishida, A.; Mikami, K. *Chem. Commun*, **1997**, 291−292. (q) Fukuzumi, S.; Suenobu, T.; Patz, M.; Hirasaka, T.; Ito, S.; Fujitsuka, M.; Ito, O. *J. Am. Chem. Soc.* **1998**, *120*, 8060−8068. (r) Akasaka, T.; Suzuki, T.; Maeda, Y.; Ara, M.; Wakahara, T.; Kobayashi, K.; Nagase, S.; Kako, M.; Nakadaira, Y.; Fujitsuka, M.; Ito, O. *J. Org. Chem.* **1999**, *64*, 566−569.

(3) Arbogast, J. W.; Darmanyan, A. P.; Foote, C. S.; Diederich, F. N.; Whetten, R. L.; Rubin, Y.; Alvarez, M. M.; Anz, S. J. *J. Phys. Chem.* **1991**, *95*, 11−12.

(4) Arbogast, J. W.; Foote, C. S. *J. Am. Chem. Soc.* **1991**, *113*, 8886−8889.

(5) Nagano, T.; Arakane, K.; Ryu, A.; Masunaga, T.; Shinmoto, K.; Mashiko, S.; Hirobe, M. *Chem. Pharm. Bull.* **1994**, *42*, 2291−2294.

(6) Tsuchiya, T.; Oguri, I.; Yamakoshi, Y.; Miyata, N. *FEBS Lett.* **1996**, *393*, 139−145.

(7) (a) Ruoff, R. S.; Tse, D. S.; Malhotra, R.; Lorents, D. C. *J. Phys. Chem.* **1993**, *97*, 3379−3383. (b) Sivaraman, N.; Dhamodaran, R.; Kaliappan, I.; Srinivasan, T. G.; Vasudeva-Rao, P. R.; Mathews, C. K. *J. Org. Chem.* **1992**, *57*, 6077−6079. (c) Sivaraman, W. A.; Tour, J. M. *J. Chem. Soc., Chem. Commun.* **1993**, 1207. (d) Heyamann, D. *Fullerene Sci. Technol.* **1996**, *4*, 509.

(8) Yamakoshi, Y.; Yagami, T.; Fukuhara, K.; Sueyoshi, S.; Miyata, N. *J. Chem. Soc., Chem. Commun.* **1994**, 517−518.

(9) Yamakoshi, Y.; Yamazaki, E.; Sueyoshi, S.; Miyata N. In *Fullerenes, Recent Advances I the Chemistry and Physics of Fullerene and Related Materials*, Vol. 5; Ruoff, R. S., Kadish, K. M., Eds.; The Electrochemical Society, Inc.: Pennington, NJ, 1998; pp 238−243.

(10) Yamakoshi, Y.; Yagami, T.; Sueyoshi, S.; Miyata, N. *J. Org. Chem.* **1996**, *61*, 7236−7237.

(11) Kai, Y.; Komazawa, Y.; Miyajima, A.; Miyata, N.; Yamakoshi,Y. *Fullerenes Nanotubes and Carbon Nanostructures* **2003**, *11*, 79−87.

(12) Sakai, A.; Yamakoshi, Y.; Miyata, N. *Fullerene Sci. Technol.* **1995**, *3*, 377−388.

(13) Sakai, A.; Yamakoshi, Y.; Miyata, N. *Fullerene Sci. Technol.* **1999**, *7*, 743−746.

(14) Tsuchiya, T.; Yamakoshi, Y.; Miyata, N. *Biochem. Biophys. Res. Commun.* **1995**, *206*, 885−894.

(15) Tsuchiya, T.; Oguri, I.; Yamakoshi, Y.; Miyata, N. *Fullerene Sci. Technol.* **1996**, *4*, 989−999.

(16) Iwata, N.; Mukai, T.; Yamakoshi, Y.; Hara, S.; Yanase, T.; Shoji, M.; Endo, T.; Miyata, N. *Fullerene Sci. Technol.* **1998**, *6*, 213−226.

(17) Yamakoshi, Y.; Sueyoshi, S.; Fukuhara, K.; Miyata, N.; Masumizu, T.; Kohno, M. *J. Am. Chem. Soc.* **1998**, *120*, 12363−12564.

(18) Tokuyama, H.; Yamago, S.; Nakamura, E.; Shiraki, T.; Sugiura, Y. *J. Am. Chem. Soc.* **1993**, *115*, 7918−7919.

(19) Boutorine, A. S.; Tokuyama, H.; Takasugi, M.; Isobe H.; Nakamura, E.; Helene, C. *Angew. Chem., Int. Ed. Engl.* **1994**, *33*, 2462−2465.

(20) Nakamura, E.; Tokuyama, H.; Yamago, S.; Shiraki, T.; Tokuyama, Y. *Bull. Chem. Soc. Jpn.* **1996**, *69*, 2143−2151.

(21) An, Y.-Z.; Chen, C.-H. B.; Anderson, J. L.; Sigman, D. S.; Foote, C. S.; Rubin, Y. *Tetrahedron*, **1996**, *52*, 5179−5189.

(22) Wasielewski, M. R.; O'Neil, M. P.; Lykke, K. R.; Pellin, M. J.; Gruen, D. M. *J. Am. Chem. Soc.* **1991**, *113*, 2774−2776.

(23) (a) Hung, R. R.; Grabowski, J. J. *J. Phys. Chem.* **1991**, *95*, 6073−6075. (b) Hung, R. R.; Grabowski, J. J. *Phys. Lett.* **1992**, *192*, 248−249. (c) Anderson, J. L.; An, Y.-Z.; Rubin, Y.; Foote, C. S. *J. Am. Chem. Soc.* **1994**, *116*, 9763−9764. (d) Williams, R. M.; Verhoeven, J. W. *Spectrochem. Acta* **1994**, *50A*, 251−254. (e) An, Y.-Z.; Viado, A. L.; Arce, M.-J.; Rubin, Y. *J. Org. Chem.* **1995**, *60*, 8330−8331. (f) Bensasson, R. V.; Bienvenue, E.; Janot, J. M.; Leach, S.; Seta, P.; Schuster, D. I.; Wilson, S. R.; Zhao, H. *Chem. Phys. Lett.* **1995**, *254*, 566−570. (g) Hamano, T.; Okuda, K.; Mashino, T.; Hirobe, M.; Aarakane, K.; Ryu, A.; Mashiko, S.; Nagano, T. *Chem. Commun.* **1997**, 21−22.

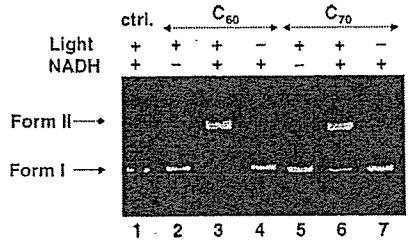

Figure 1. Photoinduced DNA cleavage by C_{60} and C_{70}. The pBR322 supercoiled plasmid was incubated with each chemical in TDC buffer for 4 h at 37 °C under irradiation with a 300-W photoreflector lamp. Lanes 1−3 and 5−6, incubation under visible light irradiation: lane 1, pBR322 DNA with 1.25% of PVP; lane 2, with 0.14 mM C_{60}; lane 3, with 0.14 mM C_{60} and 10 mM NADH; lane 5, with 0.07 mM C_{70}; lane 6, with 0.07 mM C_{70} and 10 mM NADH. Lanes 4 and 7, in the dark: lane 4, pBR322 DNA with 1.25% PVP 0.14 mM C_{60} and 10 mM NADH; lane 7 with 1.25% PVP 0.07 mM C_{70} and 10 mM NADH.

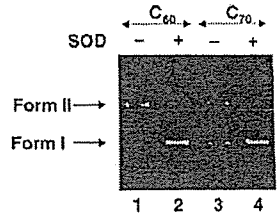

Figure 2. Effect of SOD on the photoinduced DNA cleavage by C_{60} and C_{70}. The pBR322 supercoiled plasmid was incubated with each reagent in TDC buffer for 2 h at 37 °C under irradiation with a 300-W photoreflector lamp. Lanes 1−4, PVP 1.25% incubation under visible light irradiation: lane 1, pBR322 DNA with 0.14 mM C_{60} and 10 mM NADH; lane 2, with 0.14 mM C_{60}, 10 mM NADH, and 0.04 units/mL of SOD; lane 3, with 0.07 mM C_{70} and 10 mM NADH; lane 4, with 0.07 mM C_{70}, 10 mM NADH, and 0.04 units/mL of SOD.

both photoexcited C_{60} and C_{70} cleave DNA (supercoiled form I) to give the nicked form II in the presence of NADH, a common reductant in vivo (lanes 3 and 6 for C_{60} and C_{70}, respectively). However, in the absence of NADH, neither C_{60} nor C_{70} had any effect on DNA even under photoirradiation (lanes 2 and 5 for C_{60} and C_{70}, respectively) indicating that electron transfer processes induced by the reductant are important for this activity in aqueous systems. The cleaving activity was clearly inhibited by the addition of superoxide dismutase (SOD), which quenches $O_2^{-\bullet}$ (Figure 2, lane 2 for C_{60} and lane 4 for C_{70}). This result suggested that $O_2^{-\bullet}$ is a key intermediate for DNA-cleaving activity, as shown in eq 3.

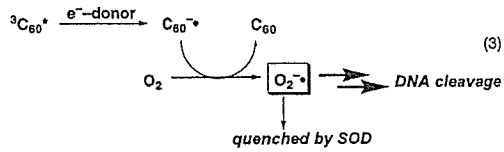

(3)

To confirm the role of $^1O_2$, the effects of $^1O_2$ stabilizers or quenchers were tested. Upon increasing the D_2O concentration in the solvent, which prolongs the lifetime of $^1O_2$, DNA cleavage was not affected, indicating the absence of a dominant role for $^1O_2$ in the DNA cleavage (data not shown). Likewise, the addition of $^1O_2$ quenchers such as sodium azide, L-histidine, and 2,5-dimethylfuran resulted in no significant decrease in the cleavage. These results support the notion that $^1O_2$, which was previously reported to be important for the photoinduced bioactivities, does not play a significant role in the expression of DNA-cleaving activity in these systems.

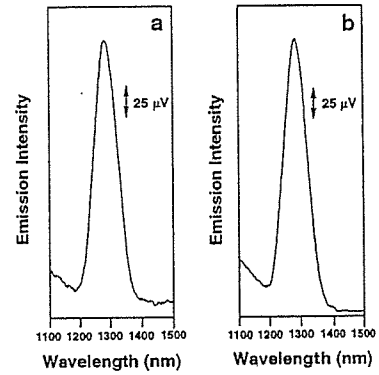

Figure 3. Near-infrared singlet oxygen luminescence emission spectra in C_{60} excited by Ar laser light at 514.5 nm with 200-mW output power. (a) 40 μM benzene solution, (b) 40 μM benzonitrile solution.

In vivo biological systems contain a similar concentration of NADH to that used in the in vitro tests employed in this paper. It is therefore possible that $O_2^{-\bullet}$ is generated in vivo and subsequently affords •OH, which is highly reactive and could directly attack DNA in the body. To compare the generation of oxyl radicals and $^1O_2$, we applied spectroscopic methods including near-infrared spectroscopy and EPR spin-trapping.

Detection of $^1O_2$. For the detection of $^1O_2$, a direct method (detection of near-infrared emission)[24] and an indirect method by EPR spin-trapping with 2,2,6,6-tetramethyl-4-piperidone (4-oxo-TEMP)[25] were employed.

A photoirradiated C_{60} solution in benzene and benzonitrile clearly showed the near-infrared $^1O_2$ luminescence emission at 1268 nm following excitation with 514.5-nm Ar laser light (Figure 3). However, we did not observe any $^1O_2$ luminescence emission in C_{60}/PVP aqueous solution. Therefore, we applied an EPR method with the spin-trapping agent 4-oxo-TEMP in order to confirm this result.

The EPR method with 4-oxo-TEMP, which reacts with $^1O_2$ to give the adduct 4-oxo-TEMPO (eq 4), was carried out with Rose Bengal, a typical water-soluble $^1O_2$ generator, as a positive control.

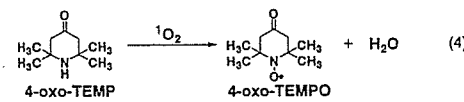

(4)

Figure 4a shows the specific signals of 4-oxo-TEMPO, which was produced by $^1O_2$ generated from photoexcited Rose Bengal, whereas no signal was detected in C_{60}/PVP aqueous solution under the same conditions (Figure 4b). This result shows that no $^1O_2$ was generated in an aqueous solution of C_{60}, even in the absence of a reductant.

Detection of $O_2^{-\bullet}$. The generation of $O_2^{-\bullet}$, which could potentially be the first-formed active oxygen species, was checked by EPR spin-trapping and the nitro blue tetrazolium method (NBT method).

5,5-Dimethyl-1-pyrroline-*N*-oxide (DMPO) was used as a spin-trapping agent for the detection of $O_2^{-\bullet}$ (eq 5). The reaction was carried out in the presence of DMSO in order to quench

(24) Arakane, K.; Ryu, A.; Takarada, K.; Masunaga, T.; Shiromoto, K.; Kobayashi, R.; Mashiko, S.; Nagano, T.; Hirobe, M. *Chem. Pharm. Bull.* **1996**, *44*, 1−4.
(25) Rion, Y.; Delmelle, M.; Van DeVorst, A. *Nature* **1974**, *263*, 442−443.

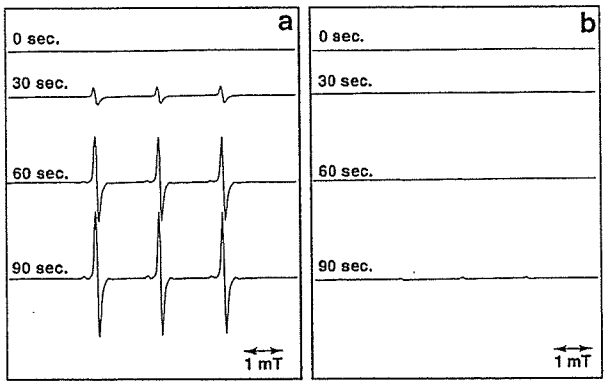

Figure 4. X-band EPR spectra of 4-oxo-TEMP adduct with $^1O_2$ generated in Rose Bengal (a) and C_{60} (b) aqueous solutions under irradiation with a 300-W photoreflector lamp. 4-Oxo-TEMP 80 mM in 50 mM phosphate buffer (pH 7). Rose Bengal or C_{60} 40 μM, PVP 0.4%. Irradiation time was 0, 30, 60, or 90 s. Experimental conditions: temperature 296 K, microwave frequency 9.394 GHz, microwave power 16 mW, field modulation 0.1 mT at 100 kHz, scan time 2 min.

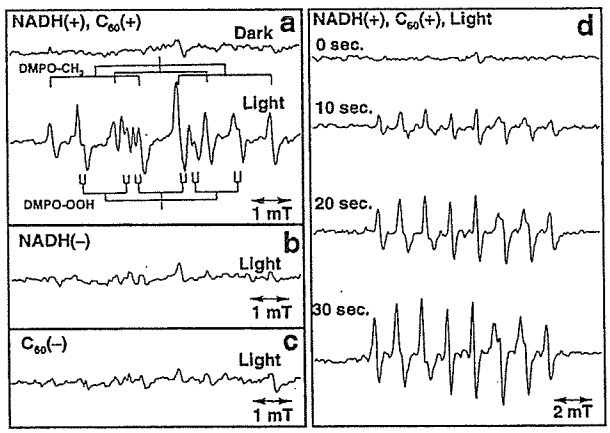

Figure 5. X-band EPR spectra of DMPO adduct with $O_2^{-\bullet}$ (a–c) and DEPMPO adduct with $O_2^{-\bullet}$ (d) generated in C_{60}/PVP aqueous solution under irradiation with a 300-W photoreflector lamp. (a–c) DMPO 0.722 M, DETAPAC 1 mM, DMSO 3.1 M, in 50 mM phosphate buffer (pH 7): (a) C_{60} 0.2 mM, PVP 2%, NADH 10 mM; (b) C_{60} 0.2 mM, PVP 2%; (c) PVP 2%, NADH 10 mM. Irradiation time: light 10 s, dark 0 s. Experimental conditions: temperature 296 K, microwave frequency 9.394 GHz, microwave power 16 mW, field modulation 0.1 mT at 100 kHz, scan time 2 min. (d): DEPMPO 50 mM, DETAPAC 1 mM, DMSO 3.1 mM in 50 mM phosphate buffer (pH 7), C_{60} 0.2 mM, PVP 2%, NADH 10 mM. Irradiation time was 0, 10, 20, or 30 s. Experimental conditions: temperature 296 K, microwave frequency 9.394 GHz, microwave power 16 mW, field modulation 0.1 mT at 100 kHz, scan time 2 min.

•OH generated under the reaction conditions used, since •OH could react rapidly with DMPO to give the adduct DMPO–OH (see eq 8), thus disturbing the spectrum of DMPO–OOH. Figure 5a shows the spectra obtained for DMPO–OOH, indicating the generation of $O_2^{-\bullet}$ from C_{60}/PVP aqueous solution in the presence of light and NADH.

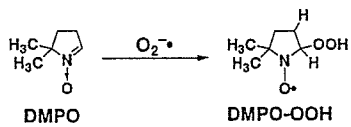

(5)

Since the lifetime of the DMPO–OOH adduct is short, 5-diethoxyphosphoryl-5-methyl-1-pyrroline-*N*-oxide (DEPMPO) was used as a spin-trapping reagent to form the more stable adduct DEPMPO–OOH (eq 6), allowing the effect of photoexposure time to be investigated. As shown in Figure 5d, the generation of $O_2^{-\bullet}$ increased in an irradiation time-dependent fashion.

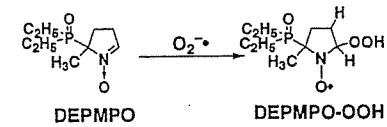

(6)

Since the quantitative detection of $O_2^{-\bullet}$ by means of spin-trapping is difficult, we employed the NBT method (eq 7) in order to quantify the amount of generated $O_2^{-\bullet}$.

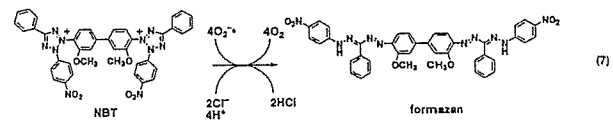

(7)

The effects of light irradiation duration, NADH concentration, and C_{60} concentration on the generation of $O_2^{-\bullet}$ were tested by the NBT method. Figure 6 shows that the generation of $O_2^{-\bullet}$ was affected by the duration of irradiation (a) and increased by the addition of NADH (b) or C_{60} (c) in a dose-dependent manner.

Detection of •OH. As reported by Cadet et al.,[26] $O_2^{-\bullet}$ itself does not cause DNA damage. However, the generation of •OH, a highly active radical which is known to cause DNA cleavage from $O_2^{-\bullet}$ via the Fenton reaction is possible under reducing conditions and the generation of •OH under the photoirradiation conditions was studied. As shown in Figure 7, the generation of •OH was detected as DMPO–OH (eq 8) in a photoexposure time-dependent manner in the presence of Fe(II).

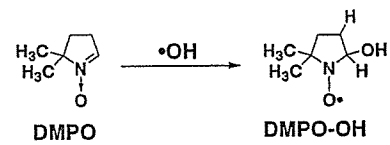

(8)

Detection of C_{60} Radical Anion ($C_{60}^{-\bullet}$). From the results described above, it is clear that $O_2^{-\bullet}$ generated under photoirradiation is converted to •OH to cause DNA cleavage, but the role of fullerenes in generating $O_2^{-\bullet}$ is less clear. Upon photoirradiation, C_{60} is known to form a long-lived triplet state which can react with electron donors, providing two possible mechanisms for the generation of active oxygen species (eq 9).

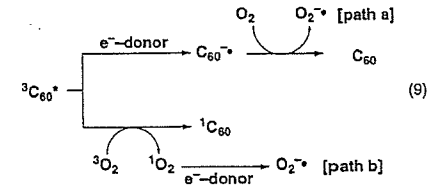

In path a, $^3C_{60}$* is reduced to $C_{60}^{-\bullet}$ which subsequently reduces O_2 to $O_2^{-\bullet}$, and in path b, $^1O_2$, which is generated by energy transfer from $^3C_{60}$* to $^3O_2$, is reduced to $O_2^{-\bullet}$. To clarify which

(26) Cadet, J.; Berger, M.; Douki, T.; Ravanat, J.-L. *Rev. Physiol. Biochem. Pharmacol.* **1997**, *131*, 1.

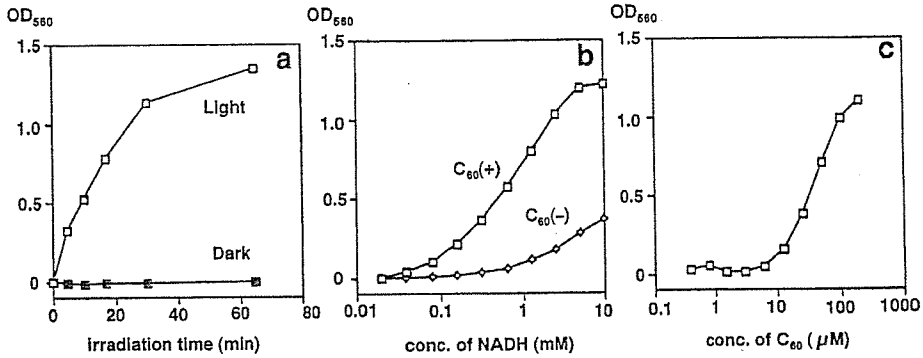

Figure 6. Photoinduced $O_2^{-\bullet}$ generation by C_{60} in PVP aqueous solution detected by the NBT method. Irradiation: 300-W photoreflector lamp at 0−5 °C. (a) Time course of $O_2^{-\bullet}$ generation with 0.2 mM C_{60}/2.5% PVP and 10 mM NADH. Light (□): under photoirradiation. Dark (■): without photoirradiation. (b) Dose-dependent effect of NADH on the photoinduced $O_2^{-\bullet}$ generation by C_{60}. Irradiation time was 30 min with 0.2 mM C_{60}/2.5% PVP (C_{60}(+)) (□) or 2.5% PVP (C_{60}(−)) (◇). (c) Dose-dependent effect of C_{60} on the $O_2^{-\bullet}$ generation by photoexcited C_{60}. Irradiation time was 30 min with 10 mM NADH.

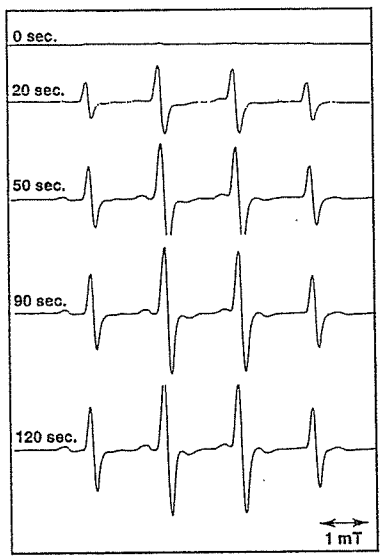

Figure 7. X-band EPR spectra of the DMPO adduct with •OH generated in C_{60}/PVP aqueous solution under irradiation with a 300-W photoreflector lamp. DMPO 0.72 M, Fe(II)-DETAPAC 0.2 mM, in 50 mM phosphate buffer, C_{60} 0.2 mM, PVP 2%, NADH 10 mM. Irradiation time: 0, 20, 50, 90, and 120 s. Experimental conditions: temperature 296 K, microwave frequency 9.394 GHz, microwave power 16 mW, field modulation 0.1 mT at 100 kHz, scan time 2 min.

pathway is most likely, we tested the detection of $C_{60}^{-\bullet}$ and the effect $^1O_2$ scavengers on the generation of $O_2^{-\bullet}$.

Since $C_{60}^{-\bullet}$ is not sufficiently stable to be detected at room temperature, we applied a convenient trapping method with 2,2,6,6-tetramethyl-4-piperidone *N*-oxide (4-oxo-TEMPO), which can react with $C_{60}^{-\bullet}$ (eq 10).

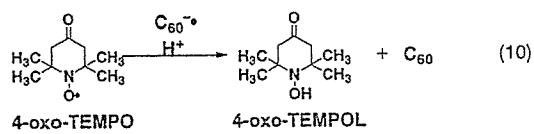

(10)

In the presence of C_{60} and NADH, a time-dependent decrease of 4-oxo-TEMPO peaks was observed under aerobic conditions (Figure 8a), whereas no reduction of the peaks was observed in the absence of NADH or C_{60} (Figure 8b and c). Importantly, no decrease of the peaks was observed in the presence of

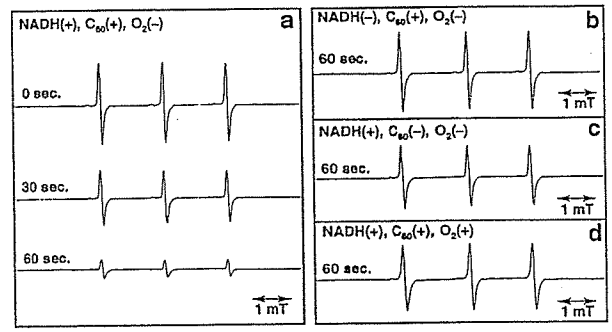

Figure 8. X-band EPR spectra of 4-oxo-TEMPO. Experimental conditions: temperature 296 K, microwave frequency 9.394 GHz, microwave power 16 mW, field modulation 0.1 mT at 100 kHz, scan time 2 min. (a) In degassed C_{60}/PVP aqueous solution under irradiation (0, 30, or 60 s) with a 300-W photoreflector lamp. 4-Oxo-TEMPO 4 μM, C_{60} 0.2 mM, PVP 2%, NADH 10 mM in 50 mM phosphate buffer (pH 7). (b) In degassed C_{60}/PVP aqueous solution without NADH under irradiation (60 s) with a 300-W photoreflector lamp. 4-Oxo-TEMPO 4 μM, C_{60} 0.2 mM, PVP 2% in 50 mM phosphate buffer (pH 7). (c) In degassed PVP aqueous solution without C_{60} under irradiation (60 s) with a 300-W photoreflector lamp. The 4-oxo-TEMPO 4 μM, PVP 2%, NADH 10 mM in 50 mM phosphate buffer (pH 7). (d) In aerobic C_{60}/PVP aqueous solution under irradiation with a 300-W photoreflector lamp. Oxo-TEMPO 4 μM, C_{60} 0.2 mM, PVP 2%, NADH 10 mM in 50 mM phosphate buffer (pH 7).

Table 1. Effect of $^1O_2$ Scavengers on Photoinduced $O_2^{-\bullet}$ Generation from Photoexcited C_{60}[a]

$^1O_2$ scavengers	OD_{560} in light	OD_{560} in dark	relative generation of $O_2^{-\bullet}$ (%)
	1.38	0.09	100
DABCO[b]	1.32	0.09	95.4
L-histidine	1.33	0.09	96.2
2,5-dimethylfuran	1.36	0.09	98.6

[a] Irradiation: 300-W reflector lamp, 30 min, 0−5 °C, with 0.2 mM C_{60}/2.5% of PVP and 10 mM NADH. [b] DABCO: 1,4-diazabicyclo[2,2,2]octane.

oxygen, indicating that $C_{60}^{-\bullet}$ transfers an electron to oxygen, rather than 4-oxo-TEMPO, to give $O_2^{-\bullet}$ (Figure 8d). This finding suggests that $O_2^{-\bullet}$ is formed via path a.

To investigate the potential that path b is operative, the effect of $^1O_2$ scavengers on $O_2^{-\bullet}$ generation was also studied by NBT the method. As shown in Table 1, there was no significant effect of $^1O_2$ scavengers on the generation of $O_2^{-\bullet}$, further suggesting that the $O_2^{-\bullet}$ generation proceeds via path a in eq 9.

Conclusions

Using spectroscopic methods (EPR spin-trapping and the NBT method), it was shown that oxyl radicals ($O_2^{-\bullet}$ and •OH) are generated from photoexcited C_{60} under physiological conditions, especially in the presence of biological reducing agents. Taking into account the results of DNA cleavage studies, we believe it is likely that reduced oxygen species ($O_2^{-\bullet}$ and •OH) are the key active species for the observed biological activities. This is in contrast to previous studies of photoexcited fullerenes, which were performed under conditions where singlet oxygen is indeed generated. However, the identification and study of the active species under physiological conditions are essential for the further development of photodynamic therapies based on fullerene and its derivatives as photosensitizers. Much work has been done on biological activities, such as enzyme inhibition or radical scavenging activity, of water-soluble fullerene derivatives. [27-34] However, the photobiological properties of C_{60} described in this paper offer a unique and a potentially promising platform for the design and development of novel therapeutic agents.

Experimental Section

EPR experiments were carried out with a JEOL JES-FE 2XG ESR spectrometer system (JEOL Ltd., Tokyo) and recorded under the following conditions: temperature 296 K, microwave frequency 9.394 GHz, microwave power 16 mW, field modulation 0.1 mT at 100 kHz, scan time 2 min. The C_{60} and C_{70} aqueous solutions were prepared with poly(vinylpyrrolidone) K30 (PVP, Wako Ltd., Tokyo), as reported previously.[8]

DNA Cleavage Assay. A super coiled plasmid DNA (pBR322, 660 μg mL^{-1}, Sigma Co. Ltd.) was diluted with 1 M Tris-HCl buffer (pH8.0) to 12.5 μg mL^{-1}. The DNA solution, fullerene solutions, and other reagent solutions (reductant or quencher) were mixed well in TDC buffer (Tris-HCl buffer with KCl and $MgCl_2$) and subjected to photoirradiation with a 300-W photoreflector lamp at a distance of 20 cm at 37 or 0−5 °C. After irradiation, an aliquot (20 μL) of the irradiated solution was mixed with bromophenol blue-glycerol solution (5 μL) and subjected to agarose gel electrophoresis (10% agarose in Timiza base EDTA (TBE) buffer, 70 V, 2 h). The gel was stained with ethidium bromide and photographed on the transilluminator for analysis of the ratio of Form I (supercoiled) and Form II (nicked).

Singlet Oxygen Detection (Near-Infrared Spectroscopy). According to the method of Arakane et al.,[35] singlet oxygen was detected by using a near-infrared spectrometer (near-infrared Ge detecter, model 403HS, Applied Detector Co., USA), cooled with liquid nitrogen, to obtain luminescence emission spectra from a test solution circulated in a quartz flow cell excited with argon laser light (Ar laser equipment, Innova 70-4, Coherenet Inc., USA) at 514.5 nm with 200-mW output power. The argon laser beam was chopped at 800 Hz by an acousto-optic modulator (A-160, Hoya Co., Japan) with a driver (110-DS, HOYA Co., Japan). The output signal from the Ge detector was led through a preamplifier (model 116, E. G. & G. Princeton Applied Research, USA) to a lock-in amplifier (model 124A, E. G. & G. Princeton Applied Research, USA), synchronized with an internal standard signal, and recorded on an XY recorder.

Singlet Oxygen Detection (EPR Spin-Trapping Method). Singlet oxygen was also detected by an EPR method using 2,2,6,6-tetramethyl-4-piperidone (4-oxo-TEMP) as a spin-trapping reagent. As a standard, $^1O_2$-generating compound Rose Bengal was employed. To a C_{60}/PVP or a Rose Bengal/PVP aqueous solution (100 μL), 250 mM phosphate buffer (50 μL), distilled water (80 μL), and 1 M 4-oxo-TEMP (20 μL) were added and mixed well under an aerobic condition. The mixed solution was introduced into a flat cell, irradiated with a 300-W photoreflector lamp at a distance of 15 cm, and immediately subjected to EPR measurement. The generation of singlet oxygen was detected as an EPR signal due to 4-oxo-TEMPO formed by the reaction of $^1O_2$ with 4-oxo-TEMP.

Detection of Superoxide Radical Anion (EPR Spin-Trapping Method). 5,5-Dimethyl-1-pyrroline *N*-oxide (DMPO) or 5-diethoxyphosphoryl-5-methyl-1-pyrroline *N*-oxide (DEPMPO) was used as a spin-trapping agent. To a C_{60}/PVP or a PVP aqueous solution (100 μL), 5 mM DETAPAC in 250 mM phosphate buffer (50 μL), DMSO (55 μL), 100 mM NADH or distilled water (25 μL), and DMPO or 625 mM DEPMPO (20 μL) were added and mixed well under an aerobic condition. The mixed solution was collected in a flat cell, irradiated with a 300-W photoreflector lamp at a distance of 15 cm, and subjected immediately to EPR measurement. The generation of $O_2^{-\bullet}$ was detected as signals due to DMPO−OOH or DEPMPO−OOH formed by the reaction of $O_2^{-\bullet}$ with DMPO or DEPMPO, respectively.

Detection of Superoxide Radical Anion (NBT Method). The generation of $O_2^{-\bullet}$ was also detected by the NBT (nitro blue tetrazolium) method as reported by Nagano et al.[36] To a solution of C_{60}/PVP or PVP (100 μL), 2.4 mM NBT (20 μL), 1 mM EDTA (20 μL), 250 mM phosphate buffer (4 μL), and a 10-fold concentrated solution of reductant (20 μL) were added and mixed well under an aerobic condition. The reaction mixture was irradiated with a 300-W photoreflector lamp at 1−5 °C and then diluted with 50 mM phosphate buffer (0.8 mL) for the measurement of OD_{560}.

Detection of Hydroxyl Radical (EPR Spin-Trapping Method). 5,5-Dimethyl-1-pyrroline *N*-oxide (DMPO) was used as a spin-trapping agent. To a C_{60}/PVP or a PVP aqueous solution (100 μL), 0.2 mM Fe(II)-DETAPAC in 250 mM phosphate buffer (50 μL), distilled water (55 μL), 100 mM NADH or distilled water (25 μL), and DMPO (20 μL) were added and mixed well under an aerobic condition. The mixed solution was collected in a flat cell, irradiated with a 300-W photoreflector lamp at the distance of 15 cm, and immediately subjected to EPR measurement. The generation of •OH was detected as signals due to DMPO−OH formed by the reaction of •OH and DMPO.

Detection of C_{60} Radical Anion (EPR Spin-Trapping Method). According to the method reported by Hadjur et al.,[37] the generation of $C_{60}^{-\bullet}$ was detected as a decrease of the signal of 4-oxo-2,2,6,6-tetamethylpyperidine *N*-oxide (4-oxo-TEMPO) due to the reaction of $C_{60}^{-\bullet}$ and 4-oxo-TEMPO to give 4-oxo-TEMPOL, which does not exhibit any radical signal. To a C_{60}/PVP or a PVP aqueous solution (100 μL), 250 mM phosphate buffer (50 μL), distilled water (5 μL),

(27) For reviews on biological properties of fullerenes, see: (a) Jensen, A. W.; Wilson, S. R.; Schuster, D. I. *Bioorg. Med. Chem.* **1996**, *4*, 767−779. (b) Wilson S. R. In *Fullerenes Chemistry, Physics, and Technology*; Kadish, K. M., Ruoff, R. S., Eds.; Wiley: New York, 2000, pp 437−466. (c) DaRos, T.; Prato, M. *Chem. Commun.* **1999**, 663−669.

(28) Isobe, H.; Sugiyama, S.; Fukui, K.; Iwasawa, Y.; Nakamura, E. *Angew. Chem., Int. Ed.* **2001**, *40*, 3364−3367.

(29) Zhou, S.; Burger, C.; Chu, B.; Sawamura, M.; Nagahama, N.; Toganoh, M.; Heckler, U. E.; Isobe, H.; Nakamura, E. *Science* **2001**, *291*, 1944−1947.

(30) Friedman, S. H.; DeCamp, D. L.; Sijbesma, R. P.; Srdanov, G.; Wudl, F.; Kenyon, G. L. *J. Am. Chem. Soc.* **1993**, *115*, 6506−6509.

(31) Sijbesma, R.; Srdanov, G.; Wudl, F.; Castoro, J. A.; Wilkins, C.; Friedman, S. H.; DeCamp, D. L.; Kenyon, G. L. *J. Am. Chem. Soc.* **1993**, *115*, 6510−6512.

(32) Schinazi, R. F.; Sijbesma, R.; Srdanov, G.; Hill, C. L.; Wudl, F. *Antimicrob. Agents Chemother.* **1993**, *37*, 1707−1710.

(33) Toniolo, C.; Bianco, A.; Maggini, M.; Scorrano, G.; Prato, M.; Marastoni, M.; Tomatis, R.; Spisani, S.; Palù, G.; Blair, E. D. *J. Med. Chem.* **1994**, *37*, 4558−4562.

(34) (a) Chiang, L. Y.; Lu, F.-J.; Lin, J.-T. *J. Chem. Soc., Chem. Commun.* **1995**, 1283. (b) Lai, Y.-L.; Chiou, W.-Y.; Chiang, L. Y. *Fullerene Sci. Technol.* **1997**, *5*, 1057.

(35) Arakane, K.; Ryu, A.; Takarada, K.; Masunaga, T.; Shinomoto, K.; Kobayashi, R.; Mashino, S.; Nagano, T.; Hirobe, M. *Chem. Pharm. Bull.* **1996**, *44*, 1−4.

(36) Umezawa, N.; Arakane, K.; Ryu, A.; Mashiko, S.; Hirobe, M.; Nagano, T. *Arch. Biochem. Biophys.* **1997**, *342*, 275−281.

(37) (a) Hadjur, C.; Wagnieres, G.; Monnier, P.; van den Bergh, H. *Photochem. Photobiol.* **1997**, *65*, 818−827. (b) Moan, J. *Acta Chem. Scand. B* **1980**, *34*, 519−521.

100 mM NADH or distilled water (25 μL), and 20 μM 4-oxo-TEMPO (50 μL) were added and mixed well under an anaerobic or aerobic condition. The mixed solution was introduced into a flat cell, irradiated with a 300-W photoreflector lamp with a distance of 15 cm, and immediately subjected to the EPR measurement.

Acknowledgment. Dedicated to Professor Dr. Masaaki Hirobe on the occasion of his 67th birthday. We thank Dr. Toshie Tsuchiya for her encouragement. We are grateful to Professor Dr. Hideo Utsumi of Kyusyu University for fruitful discussions. We also thank Professor Dr. Jeffrey W. Bode of the University of California, Santa Barbara for his advice. This work was supported in part by a Grant-in-Aid for Scientific Research on Advanced Medical Technology from the Ministry of Labor, Health and Welfare (Nano-medicine Project), Grants-in-Aid for Encouragement of Young Scientists from the Ministry of Education, Science, Sports and Culture, Japan (No. 08772053 (Y.Y.), 09772037 (Y.Y.), and 13771418 (Y.Y.)), a Grant-in-Aid for young researchers from the Ministry of Health and Welfare (Y.Y.), and a Grant-in-Aid for young researchers from the Human Science Foundation (Y.Y.).

JA0355574

ACADEMIC PRESS

Available online at www.sciencedirect.com

SCIENCE DIRECT®

Biochemical and Biophysical Research Communications 307 (2003) 80–85

BBRC

www.elsevier.com/locate/ybbrc

A novel function of connexin 32: marked enhancement of liver function in a hepatoma cell line

Jun Yang,[a] Akira Ichikawa,[b] and Toshie Tsuchiya[a,*]

[a] *Division of Medical Devices, National Institute of Health Sciences, 1-18-1 Kamiyoga, Setagaya-ku, Tokyo 158-8501, Japan*
[b] *Department of Applied Biology, Faculty of Textile Science, Kyoto Institute of Technology, Goshokaido-cho, Matsugasaki, Sakyo-ku, Kyoto 606-8585, Japan*

Received 31 May 2003

Abstract

Connexin 32 (Cx32) is the main gap junction protein in hepatocytes and plays an important role in the regulation of signal transfer and growth control in the liver by constructing gap junction channels and gap junctional intercellular communication (GJIC). In this study, the human Cx32 gene was transfected into a hepatoma cell line (HepG2) that showed aberrant expression of Cx32 and was deficient in GJIC. Cx32-transfected HepG2 not only expressed a higher level of Cx32 mRNA, but also showed increased GJIC compared with HepG2 and vector-transfected HepG2. Furthermore, the liver functions of ammonia removal and albumin secretion of HepG2 were markedly enhanced with Cx32 gene transfection. It may be expected to improve the cellular functions of the hepatoma cell line by Cx32 gene transfection and serve to develop an efficacious bioartificial liver.

Keywords: Connexin; GJIC; Liver functions; Hepatoma cell line; HepG2

Gap junctions are transmembrane channels linking neighboring cells and providING the only pathway to transfer small hydrophilic cytoplasmic metabolites less than 1000 Da, growth modulators, and second messengers between the adjacent cells, in a process known as gap junctional intercellular communication (GJIC) [1]. GJIC was suggested to play a crucial role in maintaining tissue homeostasis and controlling growth, differentiation, embryogenesis, and several functions of different tissues [2–4]. Gap junctions are composed of two hemichannels and each hemichannel consists of six connexin (Cx) protein units. At present, there are greater than 16 different Cxs in vertebrate species and expression of some Cxs is organ specific [5]. In the liver, GJIC involves at least three different connexins, Cx32, Cx26, and Cx43, depending on the cell type and cell position in the lobule [6]. In vivo, Cx32 and Cx26 are expressed in parenchymal hepatocytes and the distribution of these Cx proteins is different within the liver lobules: Cx26 preferentially localizes in the periportal zone of the lobules, whereas Cx32 appears in most hepatocytes throughout the lobules and is the major component of liver gap junctions. Furthermore, many biological activities of the liver are spatially organized within the circulatory unit and several hepatic functions differ in periportal vs. pericentral hepatocytes, including carbohydrate, lipid, and nitrogen metabolism in addition to expression of gap junctions. Recently, several studies suggested that Cx32 expression had an inhibitory effect on hepatocarcinogenesis and transfection with Cx32 cDNA inhibits the growth of hepatoma cells [7–9]. However, it was not clear whether the recovery of GJIC by transfection of Cx32 gene would enhance the liver-specific functions of hepatoma cells, which would be very important in the research of liver disease therapy.

In the last two decades, with the development of cell biology and tissue engineering, a cell-based biohybrid artificial liver (BAL) was reported to be a promising approach to support patients with acute liver failure [10]. Primary human hepatocytes would be ideal for the cellular component of BAL, but it was limited by the

* Corresponding author. Fax: +81-3-3700-9196.
E-mail address: tsuchiya@nihs.go.jp (T. Tsuchiya).

0006-291X/03/$ - see front matter © 2003 Elsevier Science (USA). All rights reserved.
doi:10.1016/S0006-291X(03)01117-3

worldwide lack of donor organs and the growth limitations of primary hepatocytes in vitro. To overcome the shortage of donor and avoid xenozoonosis risk, a hepatoma cell line (HepG2) derived from human-origin cells has good growth characteristics and less severe antigenicity, and was previously used for developing the BAL [11]. Although HepG2 maintains good liver-specific functions among hepatoma cell lines, the activities of the liver-specific functions of HepG2 were far lower compared with those of primary hepatocytes [12]. Cx32 is the major gap junction protein expressed in hepatocytes, but HepG2 is an aberrant expression of Cx32 and is deficient in GJIC. Therefore, we transfected the Cx32 gene into HepG2 and investigated the exchanges of GJIC and liver-specific functions of HepG2 in this study.

The results showed that Cx32 gene transfected in HepG2 improved the trafficking of Cx32 protein to the cytoplasmic membrane, clearly increased the GJIC, and enhanced the activities of ammonia removal and albumin secretion in the Cx32 gene transfected HepG2. This was the first finding that Cx32 could markedly enhance the liver-specific functions in a hepatoma cell line (HepG2).

Materials and methods

Cell culture. The human hepatoma cell line HepG2 from the Riken cell bank (Tokyo, Japan) was cultured at 37 °C under 5% CO_2/95% humidified air using minimum essential medium (MEM) (Nissui Pharmaceutical, Tokyo, Japan) containing 0.1 mM non-essential amino acids (NEAA) (Gibco), 10% fetal bovine serum (FBS) (Intergen, NY), and 100 U/ml penicillin–streptomycin (Gibco).

Plasmid construction and transfection. Using genomic DNA extracted from HepG2 as template, the human connexin genes were amplified by polymerase chain reaction (PCR) using primers Cx32F (5′-ATGAACTGGACAGGTTTGTAGACCTTGCTC-3′) and Cx32R (5′-TCAGCAGGCCGAGCAGCGG-3′). These amplified gene fragments were isolated and inserted into the pTARGET mammalian expression. HepG2 cells were transfected with the Cx32/pTARGET plasmid or empty vector as a control using FuGENE6 transfection reagent (Roche Diagnostics, Indianapolis, IN, USA) according to manufacturer's instructions with minor modification. After continuously culturing for two days, transfectants were selected by adding 1.3 mg/ml geneticin (Life Technologies, Frederick, MD) in the culture medium for one week. Individual transfected clones were prepared by limiting dilution cloning in 96-well plates and then culturing as for HepG2.

RT-PCR. Total RNA was isolated from cells cultured on the seventh day with TRIzol reagent according to manufacturer's instructions. The cDNA was prepared from 1 μg of total RNA by reverse transcription using a commercially available First-Strand cDNA synthesis kit (Amersham Pharmacia Biotech, Uppsala, Sweden). After proper optimization of PCR conditions, subsequent PCR was performed with 1 μl cDNA in 20 μl reaction mixture (10× PCR buffer 2 μl, dNTP 1.6 μl, each primer 2 μl, *Taq* DNA polymerase 0.2 μl, and distilled water). The conditions for RT-PCR were equilibration at 37 °C for 15 min, followed by an initial denaturation at 95 °C for 1 min, 25 cycles of 95 °C for 1 min, 60 °C for 1 min, 70 °C for 2 min, and final extension of 70 °C for 5 min. Electrophoresis of PCR products was done on 1.5% agarose gel for the visualization of connexin after staining with SYBR Green I (BioWhittaker Molecular Applications, Rockland, ME, USA). Images were captured using an image scanner and analyzed using NIH Image software. The primers used in this study were as follows:

hCx32	forward 5′-ATGAACTGGACAGGTTTGTACACCTT GCTC-3′
	reverse 5′-TCAGCAGGCCGAGCAGCGG-3′
hCx26	forward 5′-ATGGATTGGGGCACGC-3′
	reverse 5′-TTAAACTGGCTTTTTTGACTTCCC-3′

Immunocytochemical stainings. Immunocytochemical staining of Cx32 protein was performed using the VECTASTAIN ABC kit (Vector Laboratories, Inc. Burlingame, USA) following the manufacturer's instruction with some modification. Briefly, cells grown on the glass coverslips were fixed in cold pure acetone for 5 min. The acetone-fixed specimens were blocked in diluted normal blocking serum in Dulbecco's phosphate-buffered saline (PBS) at room temperature for 30 min and incubated with polyclonal rabbit anti-connexin 32 (Zymed Laboratories, San Francisco, CA) overnight at 4 °C. Protein–antibody complexes were visualized by the biotin/streptavidin/peroxidase method with diaminobenzidine tetrahydrochloride (DAB) (Vextor Laboratories, Burlingame, USA) as the chromogen. All slides were viewed with a Nikon microscope (Nikon, Japan).

Scrape-loading/dye transfer assay to measure GJIC. The scrape-loading/dye transfer (SLDT) technique was adapted after the method of El-Fouly et al. [13]. Briefly, when the cells grew into confluent monolayer cells in 35-cm dishes, cell dishes were loaded with 0.05% Lucifer Yellow (Molecular Probes, Eugene, OR, USA) in PBS (+) solution and scraped immediately with a sharp blade after rinsing with PBS (+). After incubating for 5 min at 37 °C, cells were washed with PBS (+) and monitored using a fluorescence microscope. The dye spreading distance was measured from the cell layer at the scrape to the edge of the dye front that was visually detectable.

Liver-specific function assay. The functions of the hepG2 and Cx32 transfected cells were evaluated by measuring ammonia removal and albumin secretion. For the ammonia removal activities of these cells, the cells were cultured in MEM with 5 mM ammonium chloride. After the exchange of the medium containing ammonium, the concentration of ammonia in the medium was measured at 0 and 24 h, respectively, using the indophenol method (an ammonia assay kit, Wako Pure Chemicals, Japan). The albumin secreted into the culture medium was detected by enzyme-linked immunosorbent assay kit (Exocell, Philadelphia, PA).

Statistical analysis. Student's t test was used to compare the samples. Statistical significance was represented by $p < 0.05$. Values were means ± SD. Three cultures were run for each case and all experiments were repeated at least twice.

Results

Functional GJIC in HepG2 enhanced by Cx32 gene transfection

HepG2 cells were transfected with Cx32/pTARGET plasmid DNA using FuGENE6 transfection reagent and the transfectants were obtained by selection with geneticin. Expressions of Cx mRNAs were first detected using RT-PCR (Fig. 1). As shown in Fig. 1A, Cx32 mRNA was detected and showed different levels among the HepG2, Cx32 gene- and empty vector-transfected cells, while the Cx26 mRNAs were almost not detected in all cells. The image analysis showed the level of Cx32

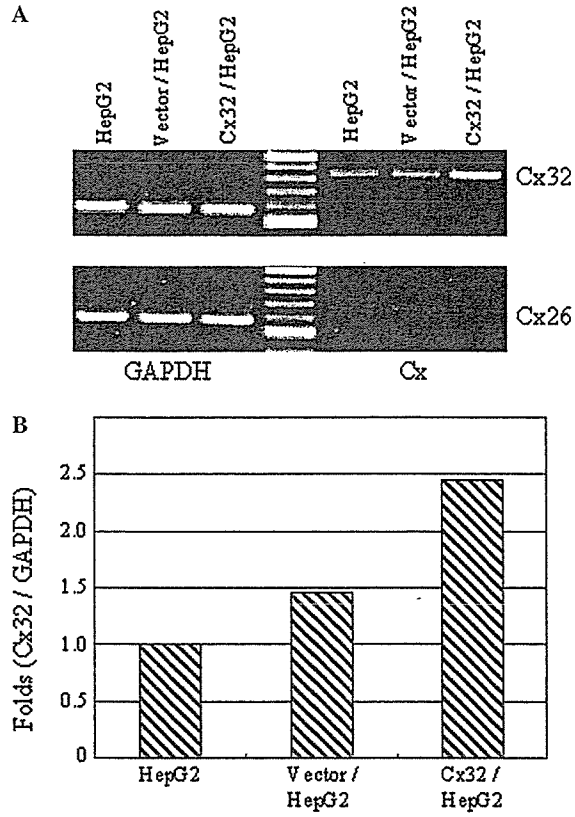

Fig. 1. Establishment of Cx32 and vector transfected HepG2. (A) RT-PCR analysis of Cx32 and Cx26 gene expression in HepG2, vector-transfected cells (Vector/HepG2), and Cx32 gene transfected cells (Cx32/HepG2). (B) Image assay of Cx32 gene expression in RT-PCR. Relative densities were standardized to that of a housekeeping gene, glyceraldehyde-3-phosphate dehydrogenase (GAPDH).

mRNA expressed in the Cx32 gene transfected cells was enhanced 2.5- and 1.7-fold in comparison with the HepG2 and empty vector transfected cells, respectively (Fig. 1B). The abilities of functional GJIC in the cells were investigated by the scrape-loading dye transfer technique. The distances of lucifer yellow spreading reflected the functional GJIC in the cells, and the longer distance of dye spreading indicates the higher functional GJIC in the cells. As shown in Fig. 2, the distance of lucifer yellow spreading in Cx32 gene transfected cells was clearly greater than those in HepG2 and empty vector transfected cells. Thus, the distance of dye spreading in Cx32 gene transfected cells was 2.8- and 1.8-fold longer than those in HepG2 and empty vector transfected cells, respectively (Fig. 3). It could be concluded that the Cx32 gene transfection not only increased the expression of Cx32 mRNA, but also significantly enhanced the functional GJIC in HepG2.

Localization of Cx32 protein before and after Cx32 gene transfection

To confirm the contribution of Cx32 protein for the formation of functional GJIC after the Cx32 gene transfection, the localizations of Cx32 protein in the cells were further observed by immunocytochemical staining. The photographs of A, B, and C in Fig. 4 show the localization of Cx32 protein in HepG2, empty vector transfected cells, and Cx32 gene transfected cells, respectively. These results demonstrated that the Cx32 protein was expressed in all the cells, but the localizations of Cx32 protein were clearly different among them. Thus, the Cx32 protein was localized in the cell borders and formed many small gap junction plaques in the Cx32 gene transfected cells, however, the Cx32 protein was limited in the cytoplasm and hardly detected the gap junction plaques in the HepG2 and empty vector transfected cells. The results in the present study suggest that the trafficking of Cx32 protein to the cell membrane in HepG2 was enhanced by Cx32 gene transfection and then increased the functional GJIC in Cx32 gene transfected cells.

Liver-specific functions in HepG2 improved by Cx32 gene transfection

For determining the effect of Cx32 gene transfection on the liver-specific functions in HepG2, the albumin secretion ability and ammonia removal activity were continuously monitored in the HepG2, empty vector transfected cells, and Cx32 gene transfected cells, respectively (Fig. 5). Albumin secretion, which was used as a marker for protein synthesis in the liver, showed greater amounts of albumin detected in Cx32 gene transfected cells than HepG2 and empty vector transfected cells (Fig. 5A). Furthermore, ammonia removal activity, which represents the detoxification potentiality of the liver, was significantly higher in the Cx32 gene transfected cells than HepG2 and empty vector transfected cells during the 14 days of culture with 5 mM ammonium chloride (Fig. 5B). It was suggested that the small molecular ammonium was effectively eliminated through the gap junctional channels formed by Cx32 in HepG2. The enhancement of liver-specific functions of HepG2 was suggested to relate to the increasing functional GJIC by Cx32 gene transfection.

Discussion

HepG2 cells, a human hepatoma cell line, are deficient in GJIC due to the aberrant expression of Cx32 and low expression of Cx26. In in vivo and in vitro models, low or no functional GJIC was observed in various kinds of hepatocarcinoma and hepatoma, which was suggested to be involved in the malignant phenotype of cancer and tumor cells [14]. In vivo, normal rodent hepatocytes express Cx32 and Cx26, but only Cx32 expression is constant across the liver lobule [6]. Thus, liver gap junction channels composed of Cx32 are

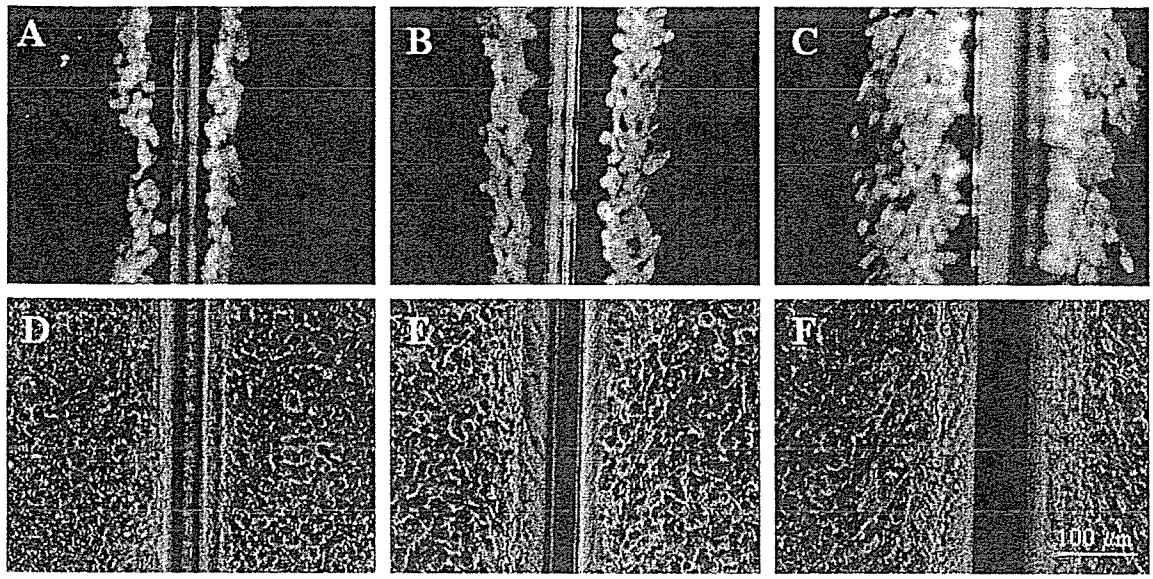

Fig. 2. Fluorescent (A–C) and phase-contrast (D-F) photographs of HepG2 (A and D), vector-transfected HepG2 (Vector/HepG2) (B and E), and Cx32-transfected HepG2 (Cx32/HepG2) (C and F) in the assay of scrape loading and dye transfer (SLDT), same scale in (A–F).

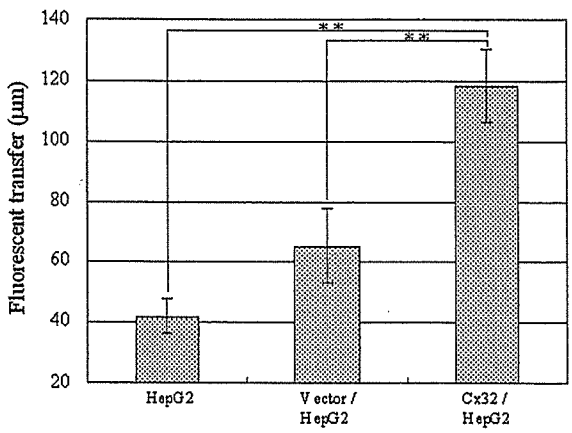

Fig. 3. Functional GJIC in HepG2, vector-transfected HepG2 (Vector/HepG2), and Cx32-transfected HepG2 (Cx32/HepG2) measured by the SLDT method at the seventh day of culture. Values are expressed as means from 20 determinations (**$P < 0.01$).

suggested to be important to maintain the normal phenotype of hepatocytes. Therefore, to reduce malignant phenotype and improve liver-specific functions in HepG2, we transfected human Cx32 gene into HepG2 to enhance functional GJIC.

The results of the RT-PCR and SLDT assay in the present study showed that the levels of Cx32 mRNA expressed in Cx32 gene transfected cells were increased greater than twofold compared with HepG2 (Fig. 1) and the functional GIJC was also markedly enhanced by Cx32 gene transfection in HepG2 (Figs. 2 and 3). Analyses of chemically induced rat liver tumors suggest that Cx32 gene is rarely mutated in these tumors but the expression of the Cx32 protein is often reduced or the Cx32 protein is abnormally localized in these cells [15]. In the present study, although the Cx32 protein expression by Western blotting assay showed almost no change even after Cx32 gene transfection (data not shown), a clear difference in the localization of Cx32 protein was observed between before and after Cx32

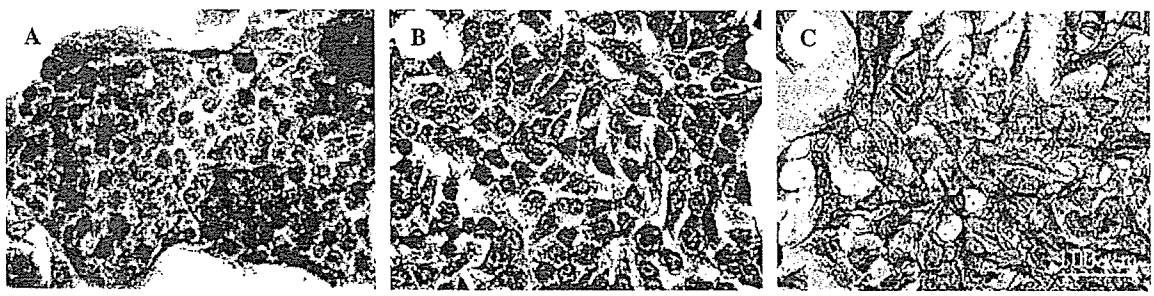

Fig. 4. Localization of Cx32 protein in HepG2 (A), vector-transfected HepG2 (B), and Cx32-transfected HepG2 (C). More gap junction plaques were detected in Cx32 gene transfected cells (arrow) than HepG2 and empty vector transfected cells. Immunocytochemical staining of Cx32 protein was performed with a Vectastain ABC Kit and polyclonal rabbit anti-connexin 32, same scale in (A–C).

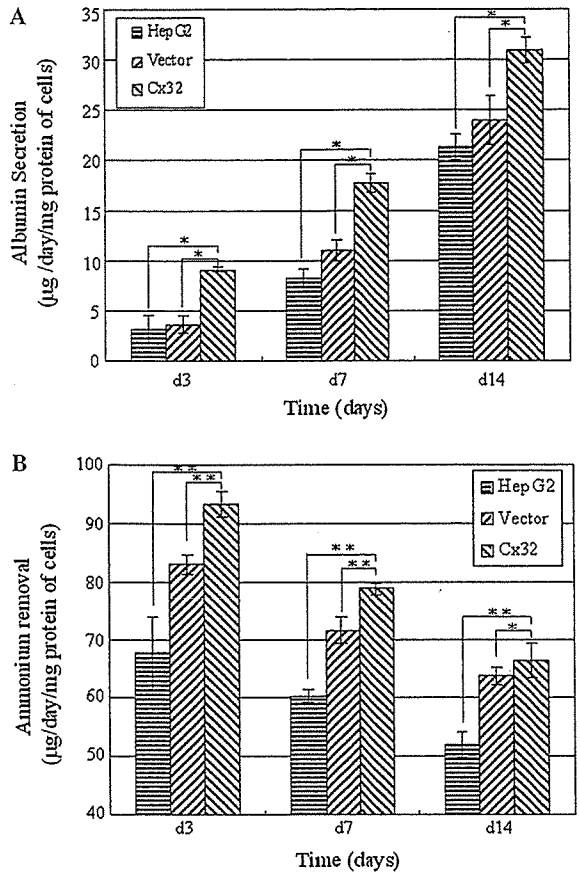

Fig. 5. Liver functions of albumin secretion (A) and ammonia removal (B) of HepG2, vector-transfected HepG2, and Cx32-transfected HepG2 examined on the 3rd, 7th, and 14th day of culture (*$P < 0.05$, **$P < 0.01$).

gene transfection in HepG2 by immunocytochemical stainings (Fig. 4). The majority of Cx32 protein was localized in the cell borders and formed small gap junction plaques in the Cx32 gene transfected cells, whereas it was limited to the cytoplasm and nucleus before Cx32 gene transfection. Furthermore, the morphologies of the cells showed that Cx32 gene transfected cells grew as a monolayer with the spreading cell shape, while the HepG2 grew as clusters with the spherical cell shape. Cx protein expression, gap junction assembly, and its function are controlled by the transcription, translation, and post-translational modification. In addition, recent studies have suggested that they are also associated with tight junction components and elements of the cytoskeleton [16–18]. Although the precise role of the cellular morphology in gap junctional channel formation between the cells is not clear at present, the results of the present study suggest that the trafficking, assembly of Cx32, and functional GJIC in the cellular membrane are enhanced by forced expression of Cx32 in HepG2.

Furthermore, Cx32 gene transfection into HepG2 markedly enhanced the liver-specific functions of ammonia removal and albumin secretion with accompanying increase in the functional GJIC (Fig. 5). Ammonia removal activity and albumin secretion ability are typical differentiated functions of the liver, but these functions in HepG2 were significantly lower than those of hepatocytes in vivo. The defect in albumin production was reported to be due to the reduction or absence of albumin gene transcription in some hepatoma cells, and the structure of the albumin gene was detected in all MH1C1, FAO, and 3924A rat hepatoma cells, but a different albumin expression was found to correlate well with methylation state of the albumin gene [19]. The results in the present study showed that the transcription of albumin gene in HepG2 may be enhanced with the increase in the functional GJIC by Cx32 gene transfection, and the albumin production was increased (Fig. 5A). In addition, the studies of ammonia removal activity in HepG2, Cx32 gene transfected cells, and vector transfected cells showed that urea was not detected in the culture media of all cells, and the ability of ammonia removal was higher in the absence than the presence of 4 mM glutamine in the media in all cells (data not shown). In the intact liver, the two major ammonia-detoxification systems, urea and glutamine synthesis, are anatomically present in periportal and pericentral hepatocytes, respectively [20]. In functional terms, this organization represents the sequence of a periportal low-affinity but high-capacity system (ureogenesis) and a pericentral high-affinity system for ammonia detoxification (glutamine synthesis). Therefore, the present results suggested that HepG2 eliminated ammonia via the high-affinity pathway of glutamine synthesis, and the capacity enhanced with the increase in the functional GJIC by forced expression of Cx32, which could be similar to the characters of Cx32 high-expressional pericentral hepatocytes. Furthermore, glutamine is an essential nutrient as a major source of energy and nitrogen for mammalian cells, which would be useful for the development of bioartificial liver. These results showed that the ammonium metabolic activity and albumin secretion in HepG2 were related to the functional gap junctional channel composed of Cx32 proteins. Other studies reported distinct biological roles of the highly homologous Cx proteins in correlations of Cx mRNA isoform expression with the degree of hepatic cellular differentiation (in RLC, FTO.2B, and WB-F344 cell lines), and suggested that Cx gene expression may be a marker of hepatic development: as hepatocytes differentiate, the proportions of Cx43 and then Cx26 mRNA decrease while that of Cx32 mRNA increases [21]. Moreover, the diffusion of second messengers through gap junction channels composed of Cx32 in liver is suggested to be a major determinant for the establishment of metabolic coupling between neighboring hepatocytes and for the proper distribution of signals involved in the promotion of liver-specific functions.